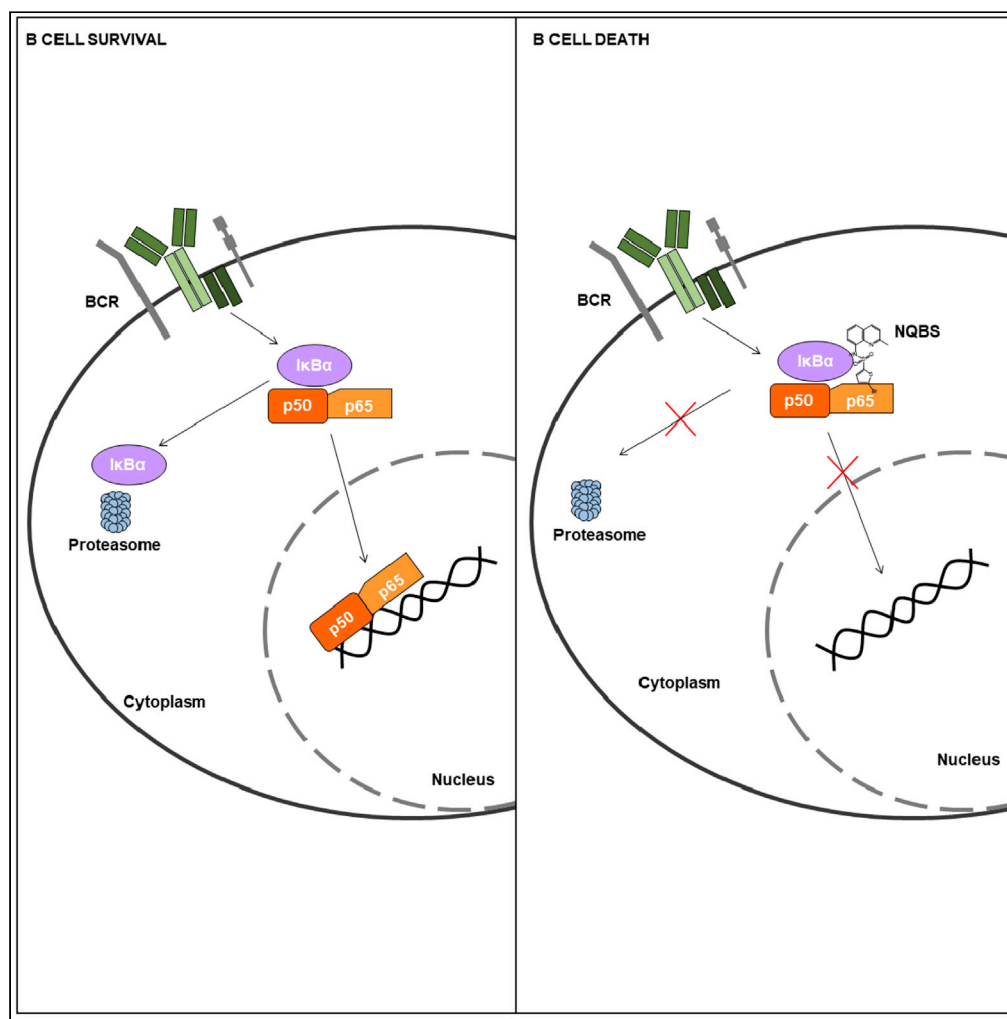


Article

N-quinoline-benzenesulfonamide derivatives exert potent anti-lymphoma effect by targeting NF- κ B



Matko Kalac,
Michael Mangone,
Alison
Rinderspacher, ...,
Andrea Califano,
Donald W. Landry,
Owen A.
O'Connor

matko.kalac@mssm.edu

HIGHLIGHTS

NQBS inhibits NF- κ B translocation to the nucleus by stabilizing I κ B α -p50-p65 trimer

Exclusion of the NF- κ B from the nucleus of the lymphoma cell leads to its rapid death

Preliminary *in vivo* data suggest NQBS to be efficacious and tolerable

Kalac et al., iScience 23,
101884
December 18, 2020 © 2020
The Author(s).
[https://doi.org/10.1016/
j.isci.2020.101884](https://doi.org/10.1016/j.isci.2020.101884)

Article

N-quinoline-benzenesulfonamide derivatives exert potent anti-lymphoma effect by targeting NF- κ B

Matko Kalac,^{1,2,3,11,*} Michael Mangone,^{1,2} Alison Rinderspacher,^{1,4} Shi-Xian Deng,^{1,4} Luigi Scotto,^{1,2} Michael Markson,³ Mukesh Bansal,^{1,5,6} Andrea Califano,^{1,6,7,8,9} Donald W. Landry,^{1,4} and Owen A. O'Connor^{1,2,10}

SUMMARY

We previously identified the N-quinoline-benzenesulfonamide (NQBS) scaffold as a potent inhibitor of nuclear factor- κ B (NF- κ B) translocation. Now, we report the structure-activity relationship of compounds with the NQBS scaffold in models of diffuse large B-cell lymphoma (DLBCL). We identified CU-O42, CU-O47, and CU-O75 as NQBS analogs with the most potent cytotoxic activity in DLBCL lines. Their anti-lymphoma effect was mediated by NF- κ B sequestration to the cytoplasm of DLBCL cells. Internal Coordinates Mechanics analysis suggested direct binding between CU-O75 and I κ B α /p50/p65 which leads to the stabilization of the NF- κ B trimer. A whole cellular thermal shift assay confirmed direct binding of the NQBS to I κ B α , an inhibitory component of the I κ B α /p50/p65 trimer. Lymphoma cell line sequencing revealed CU-O75 induced downregulation of NF- κ B-dependent genes and DeMAND analysis identified I κ B α as one of the top protein targets for CU-O75. CU-O42 was potent in inhibiting tumor growth in two mouse models of aggressive lymphomas.

INTRODUCTION

Diffuse large B-cell lymphoma (DLBCL) is the most common type of non-Hodgkin lymphoma and represents an aggressive malignancy that is treated with combination immuno-chemotherapy. Large studies have shown that standard of care first-line therapy (rituximab, cyclophosphamide, doxorubicin, vincristine and prednisone - R-CHOP) results in long-term survival of approximately 50–60% of patients (Teras et al., 2016; Coiffier et al., 2002). For patients with refractory and relapsed disease, second-line salvage regimens with autologous stem cell transplant can provide a cure in up to 50% of patients. However, those patients with refractory disease and disease that relapses early after first-line treatment have particularly poor outcomes (Gisselbrecht et al., 2010). While immunotherapy-based approaches including bispecific T-cell engagers (Viardot et al., 2016) and chimeric antigen receptor T cells (CAR T) (Neelapu et al., 2017; Schuster et al., 2019) have shown impressive response rates in previously treated patients with DLBCL, continued relapses following these treatments necessitate the search for other novel treatment options with acceptable toxicity profiles, particularly in the elderly population (Coiffier et al., 2002).

DLBCL is a heterogeneous group of lymphomas defined by genetic and diagnostic markers which stratify patients into distinct prognostic groups. Historically, patients with activated B-cell (ABC) subtype of DLBCL have poorer outcomes compared to those with germinal center (GCB)-like DLBCL (Swerdlow et al., 2008; Alizadeh et al., 2000; Shaffer et al., 2012). The inherent resistance of the ABC DLBCL to standard treatment options is due, in part, to multiple genetic alterations involving proteins within the B-cell receptor (BCR), CD40L/CD40 and TLR/IL1R pathways, including CD79A and B, CARD11, MYD88, and A20, which result in constitutive nuclear factor- κ B (NF- κ B) activation (Pasqualucci, 2013; Davis et al., 2010; Ngo et al., 2010; Kato et al., 2009; Lenz et al., 2008). Addition of lenalidomide or ibrutinib to R-CHOP showed promising results in abrogating adverse outcomes associated with the ABC disease subtype (Nowakowski et al., 2015; Younes et al., 2014), and a recent report of a phase III study in non-GCB subtypes of DLBCL showed a modest benefit in adding ibrutinib to R-CHOP in patients younger than 60 years. Older patients treated with the same regimen experienced higher toxicity and further studies are needed (Younes et al., 2019).

¹Department of Medicine, Columbia University Irving Medical Center, New York, NY, USA

²Center for Lymphoid Malignancies, Columbia University Irving Medical Center, New York, NY, USA

³Department of Hematology and Oncology, Tisch Cancer Institute, Icahn School of Medicine at Mount Sinai, 1 Gustave L. Levy Place, New York, NY 10029, USA

⁴Department of Nephrology, Columbia University Irving Medical Center, New York, NY, USA

⁵Psychogenics Inc., Paramus, NJ, USA

⁶Department of Systems Biology, Columbia University Irving Medical Center, New York, NY, USA

⁷Department of Biomedical Informatics, Columbia University, New York, NY, USA

⁸Department of Biochemistry and Molecular Biophysics, Columbia University, New York, NY, USA

⁹J.P. Sulzberger Columbia Genome Center, New York, NY, USA

¹⁰Division of Hematology and Oncology, University of Virginia Cancer Center, Charlottesville, VA, USA

¹¹Lead Contact

*Correspondence:

matko.kalac@mssm.edu

<https://doi.org/10.1016/j.isci.2020.101884>



NF- κ B is one of the most ubiquitously implicated transcription factors in lymphoma development. NF- κ B family consists of five proteins (p105/50, p100/p52, c-Rel, RelA/p65, and RelB) that regulate expression of >400 transcriptional target genes (Brasseres and Baldwin, 2006; Dutta et al., 2006; Luo et al., 2005). These encode for transcription factors, regulators of apoptosis, cell surface receptors, and early response genes, among others (Karin, 2006), that play a central role in the dysregulated growth and survival of most cancer cells.

Pathways leading to NF- κ B activation are divided into the canonical (κ B dependent, via TNF α , IL-1, and LPS), non-canonical (κ B independent, via CD40/CD40L), and atypical (genotoxic stress, hypoxia, and reactive oxygen species) pathways, which all ultimately lead to the nuclear translocation of active NF- κ B subunits (Ghosh and Baltimore, 1990; Ghosh et al., 1998; Oeckinghouse et al., 2011). Over-expression and constitutive activation of NF- κ B is thought to be one of the central drivers in cancer biology including lymphomagenesis (Ghosh and Karin, 2002; Derudder et al., 2003; Xiao et al., 2001; Coope et al., 2002; Claudio et al., 2002; Dejardin et al., 2002). Identification of pharmacologic strategies to inhibit the activation of target NF- κ B genes has thus become a key area of investigation (Herrington et al., 2015; Baud and Marin, 2009).

While over 700 inhibitors of the NF- κ B signaling pathway have been experimentally identified (Gilmore and Herscovitch, 2006), very few of them have made it to the clinic. The Food and Drug Administration approved agents used in oncology and rheumatology, which act by modulating NF- κ B indirectly, and include proteasome inhibitors [bortezomib (Kane et al., 2003) and carfilzomib (Herndon et al., 2013)], disease-modifying anti-rheumatic drugs (sulfasalazine and mesalamine), and anti-cytokine biologics [anakinra, infliximab, and adalimumab (Gilmore and Herscovitch, 2006)]. Hence, there is an urgent need for higher specificity, targeted therapeutic options to inhibit the NF- κ B cascade.

High-throughput screening performed at the Columbia University and National Institutes of Health (NIH) identified small-molecule inhibitors of the NF- κ B pathway: *N*-quinoline-benzenesulfonamides (NQBSs) (Xie et al., 2008), which were able to block nuclear translocation of NF- κ B in human umbilical vein endothelial cells, were stimulated by TNF α . Here, we present data from structure-activity relationship (SAR) analyses, within preclinical models of DLBCL, that confirm the NF- κ B-specific activity of NQBS analogs, leading to potent cytotoxic and pro-apoptotic effect in DLBCL models. This effect is mediated by direct binding of the NQBS analogs to κ B α , which stabilizes its interaction with NF- κ B dimers and sequesters them in the cytoplasm.

RESULTS

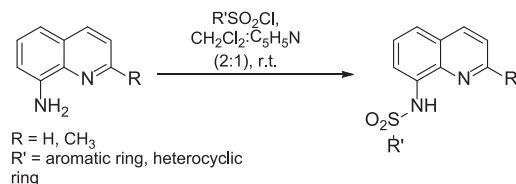
Chemical Synthesis and Lead Compound Identification

We performed SAR analysis on the previously identified NQBS structure aiming to identify derivatives with potent *in vitro* lymphoma cytotoxicity, while retaining their inherent NF- κ B nuclear exclusion properties, an essential characteristic of the NQBS scaffold. All of the initially described compounds, as well as those that were additionally synthesized, were screened by an algorithm, validating three key aspects of an NF- κ B-targeted compound: an ATP-based luminescence cell viability assay (anti-lymphoma effect), immunofluorescence microscopy (NF- κ B subunit nuclear exclusion), and chemiluminescence-based electrophoretic mobility shift assay (EMSA) (inhibition of NF- κ B subunit DNA binding) in 2 DLBCL cell lines (OCI-Ly1 – GCB DLBCL and OCI-Ly10 – ABC DLBCL). All of the derivatives tested in this manner are listed in Tables S1–S8. A general approach to NQBS synthesis is shown in Figure 1A. The chemical structures of three of the active compounds are shown in Figure 1B (CU-O42, CU-O47, and CU-O75), while the fourth structure represents the inactive analog molecule CU-O102, used in subsequent experiments as a negative control. Spectral data for these 4 compounds are presented in Figure S1.

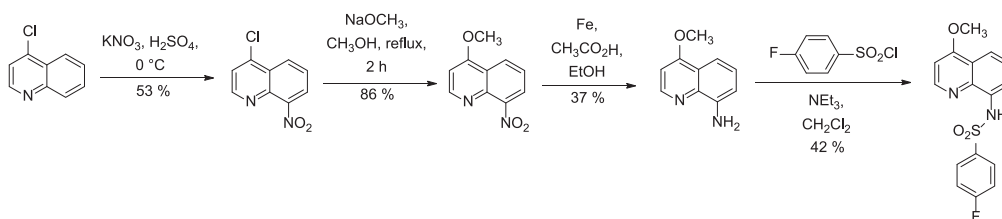
The effect of NQBS analogs in inducing cytotoxicity in lymphoma cell lines is shown via heatmap in Figure 2A. Figure S2 shows the growth inhibition IC₅₀ values of CU-O75 across a spectrum of lymphoma lines including DLBCL and mantle cell lymphoma (MCL). CU-O75's IC₅₀ values in these lines ranged between 0.75 and 1.5 μ M. Neither of the active compounds exhibited clear differences in observed growth inhibition between the ABC and GCB DLBCL subtypes as shown in summary graph in Figure 2B. Similarly, lack of DLBCL subtype specificity was previously reported with another class of NF- κ B-targeted compounds (κ B kinase [IKK] inhibitors) in the cell line models tested (Deng et al. 2015). NQBS-related compounds were potent inducers of apoptosis as shown in Figures 2C and 2D, and no clear difference was again observed in the induction of apoptosis between cell lines representing ABC and GCB DLBCL subtypes.

A

Scheme 1.



Scheme 2.



B

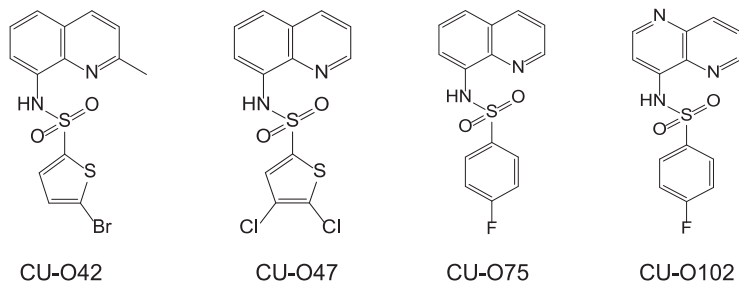


Figure 1. NQBS chemical structure

(A and B) (A) General synthetic pathways for the preparation of NQBS; (B) chemical structure of representative compounds (CU-O42, CU-O47, CU-O75, and CU-O102)

Next, we performed a drug washout experiment in order to identify the duration of incubation needed for the biologic effect of NQBS-related compounds in DLBCL lines. OCI-Ly1 and OCI-Ly10 were incubated with CU-O47 and CU-O75 for 1 and 3 h, respectively (pulse exposure), after which the cells were washed and incubated in NQBS-free medium. Cell viability was analyzed at 24, 48, and 72 h, as shown in Figure S3. In the samples treated with 1h pulse, lymphoma growth inhibition was observed only at the highest concentration of CU-O47 and CU-O75, resulting in a significant right shift of the concentration:effect curve compared to continuously treated cells. Three-hour treatment with CU-O75 abrogated this difference proving that NQBSs yield their biologic effect on DLBCL cells in a remarkably rapid manner. Three-hour treatment with CU-O47 had a similar effect, displaying a concentration:effect curve approaching that of the continuous treatment group. Again, neither CU-O75 or CU-O47 exhibited selectivity for the ABC DLBCL.

NQBS-Mediated Inhibition of NF- κ B Nuclear Translocation

While the initial discovery of NQBS-related compounds was made in a TNF α -stimulated human umbilical vein endothelial cell line (HUVEC) model, we sought to explore the effect of CU-O75, CU-O42, and CU-O47 in a cellular model with constitutive NF- κ B activation, without TNF α stimulation. OCI-Ly10 is an ideal model as this cell line is derived from a patient with ABC DLBCL and has A20 and MYD88 mutations resulting in NF- κ B overexpression (Ma et al., 2015). As shown in Figure 3A, untreated and TNF α -unstimulated

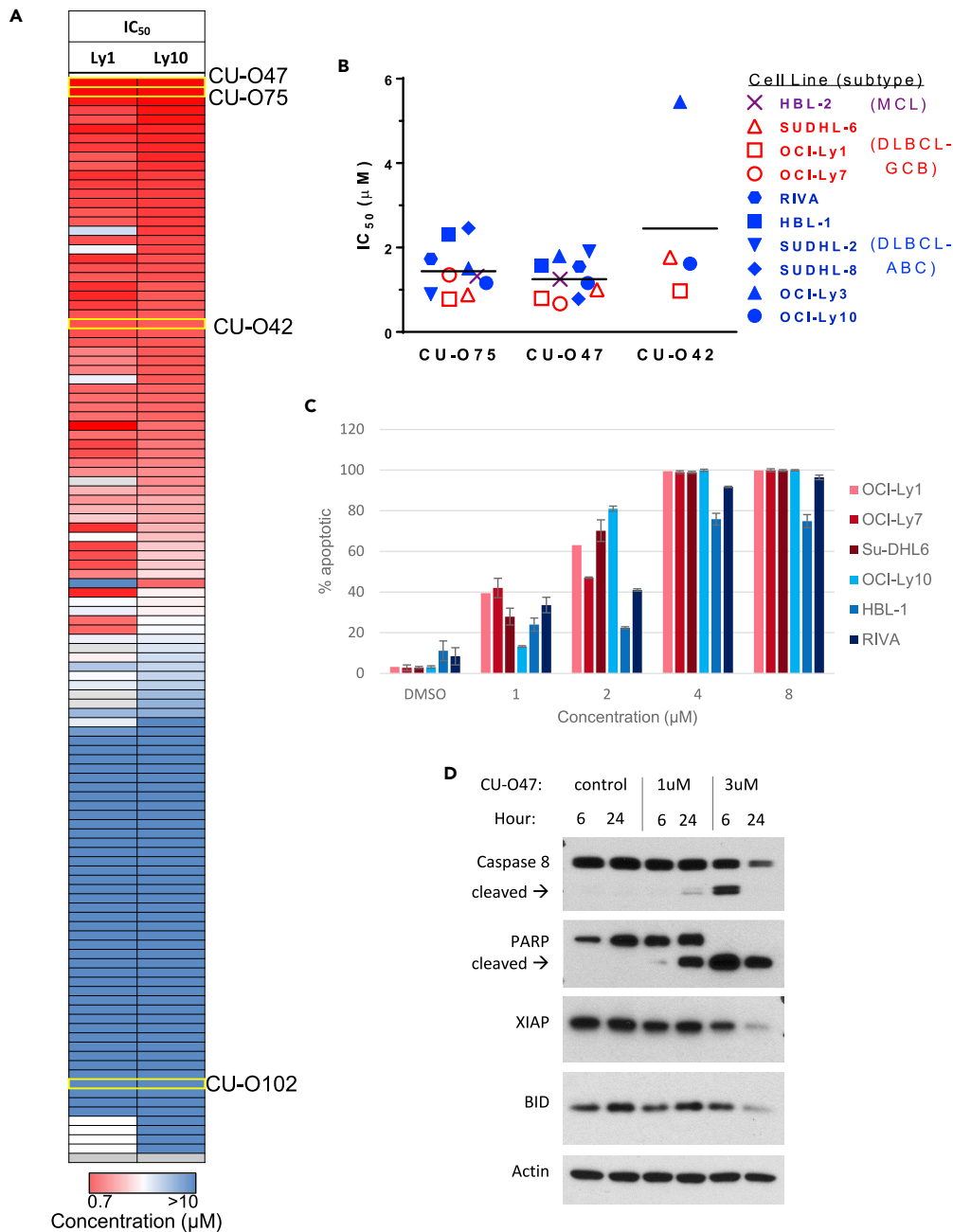


Figure 2. Anti-lymphoma activity of NQBS

(A) Heatmap representing the activity of NQBS in inducing cell growth inhibition in 2 DLBCL lines (OCI-Ly1 and OCI-Ly10), measured by IC₅₀ values using an ATP-based luminescence viability assay at 72 h. Representative compounds (CU-O42, CU-O47, CU-O75, and CU-O102) are highlighted. All of the experiments were performed in triplicates and repeated at least twice. (B) NQBSs induce growth inhibition in lymphoma cell lines as measured by IC₅₀ in an ATP-based luminescence viability assay at 24 h. Cell lines are color labeled as GCB DLBCL (red), ABC DLBCL (blue), and MCL (purple). All of the experiments were performed in triplicates and repeated at least twice. (C) NQBSs induce apoptosis in lymphoma cell lines. PI and Yo-Pro flow cytometric analysis of CU-O42 effect in DLBCL cell lines at 24h. Cell lines are color labeled as GCB DLBCL (red) and ABC DLBCL (blue). Values represent means expressed as percentages compared with the untreated control; error bars represent SD. All of the experiments were performed in triplicates and repeated at least twice. (D) Immunoblot analysis in OCI-Ly10 cell line treated with CU-O47 shows a cleavage of Caspase 8 and PARP, as well as a decrease in the level of XIAP and BID as markers of apoptosis induction.

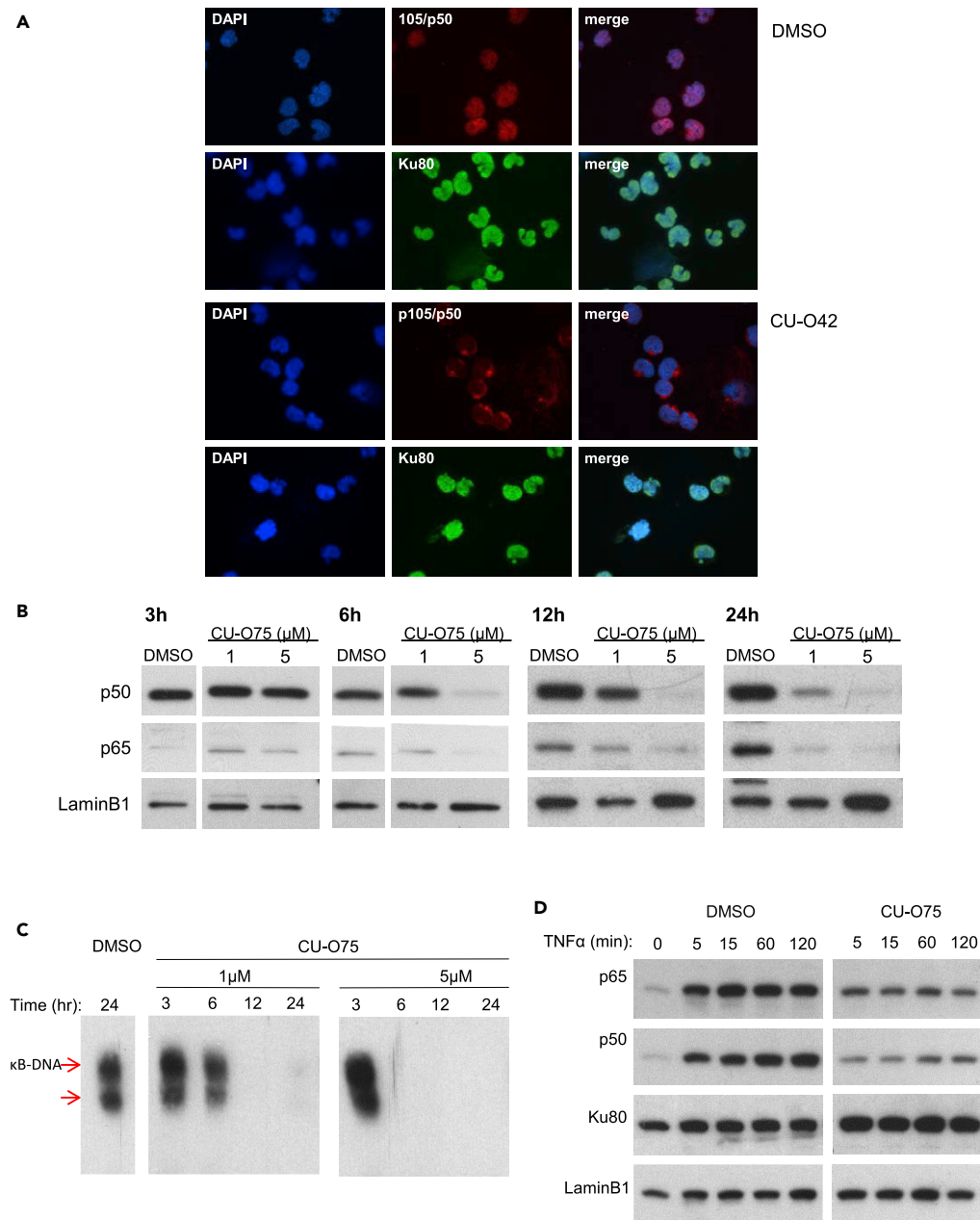


Figure 3. Inhibition of NF- κ B translocation

(A) Immunofluorescent microscopy analysis in OCI-Ly10 following a 6h incubation with CU-O42 shows p50 sequestration in the cytoplasm. This effect is NF- κ B specific as it does not affect other transcription factors capable of translocating between the cytoplasm and the nucleus (e.g. Ku80)

(B) Immunoblotting analysis confirms decreased nuclear levels of p50 and p65 following CU-O75 treatment in OCI-Ly10 cells. A superfluous lane was cut out from the panels representing 3h and 6h treatment with CU-O75. This lane was an additional sample treated with TNF α . Since the effect of TNF α occurs quickly (within 5 min) and is lost by the 3h time point, this lane provided irrelevant information

(C) Chemiluminescence-based electrophoretic mobility shift assay (EMSA) analysis of the effect NQBSs have on direct NF- κ B binding to DNA. There was a decreased binding of NF- κ B to DNA following incubation of OCI-Ly10 cells with CU-O75. This effect was both time and concentration dependent. Three superfluous lanes were cut out from this image. As per manufacturer's instruction, we included 3 additional assay controls including: (1) a control without the lysate; (2) a control with excess unlabeled probe at 24h; and (3) untreated control. These additional lanes provided quality control but were irrelevant to the data.

Figure 3. Continued

(D) NQBS effect on nuclear levels of p50 and p65 in Jurkat cells following stimulation with TNF α . As early as 5 min after the addition of TNF α to the cell culture, there was a significant increase in nuclear levels of p50 and p65. A 4-h pre-incubation with CU-O47 inhibited TNF α -induced nuclear localization of p50 and p65. Incubation with either TNF α alone or both TNF α and CU-O75 did not have any effect on other transcription factors.

OCI-Ly10 cells have p50 (red) present in the nucleus (top row, middle and right images). Treatment with CU-O42 for 6h results in p50 sequestration into the cytoplasm (third row, middle and right images). NQBS-related compounds do not affect nuclear localization of other transcription factors (e.g., Ku80 shown in green). Next, we wanted to analyze this effect on a quantitative protein level. We treated OCI-Ly10 cells with increasing concentrations of CU-O75 and analyzed the total nuclear levels of p50 and p65 proteins. Decrease in nuclear levels of both p50 and p65 was observed in both time and concentration-dependent manners (Figure 3B). We also used a EMSA to analyze the effect NQBSs have on direct NF- κ B binding to DNA. As shown in Figure 3C, together with the observed decrease in the nuclear NF- κ B, there was also decreased binding of NF- κ B to DNA. Again, this CU-O75-mediated effect was both time and concentration dependent.

Finally, we wanted to validate the data that led to the NQBS discovery in a lymphoma model. For this, we used a Jurkat cell line, with no constitutive overactivation of NF- κ B, similar to the HUVEC line requiring TNF α stimulation for NF- κ B translocation to the nucleus. Figure 3D shows the effect on nuclear levels of p50 and p65 following stimulation with TNF α . As early as 5 min after the addition of TNF α to the cell culture, there was a significant increase in nuclear levels of p50 and p65. A 4-h pre-incubation with CU-O47 inhibited TNF α -induced nuclear localization of p50 and p65. Incubation with either TNF α alone or both TNF α and CU-O75 did not have any effect on other transcription factors (e.g., Ku80).

Mechanistic Elucidation of NQBS-Mediated NF- κ B Inhibition

We then explored possible mechanism of NQBS-mediated inhibition of NF- κ B. First, we wanted to rule out conventional mechanisms known to affect NF- κ B subunit localization, as induced by proteasome and IKK inhibition. We investigated the activity of NQBS-related compounds on proteasome function. Graphs in Figure S4A represent the effect of NQBS on all three functions of the proteasome. While positive controls bortezomib and carfilzomib effectively inhibited the chymotrypsin-like activity of the proteasome, the NQBS-related compounds exerted minimal to no effect on chymotrypsin-like, trypsin-like, and caspase-like proteolytic activities of cellular proteasomes. This effectively proved that CU-O42, CU-O47, and CU-O75 were not proteasome inhibitors.

We also tested NQBS in the DISCOVERx kinome screen where CU-O42 and CU-O75 failed to inhibit any of the 403 kinases screened. Importantly, they did not inhibit any of the IKK family kinases. Furthermore, phosphorylated I κ B α levels were not affected by treatment of OCI-Ly1, OCI-Ly10, or HBL-1 cells with CU-O42 (Figure S4B), confirming NQBS-related compounds did not act via IKK inhibition and were likely not protein kinase inhibitors.

Having proven that NQBSs do not act via established mechanisms, we sought to elucidate the novel mechanism by which NF- κ B pathway inhibition may arise. For this, we focused on potential binding of these compounds to one or more members of the NF- κ B protein family. To test this hypothesis, we used Internal Coordinate Mechanics software to identify potential binding sites between CU-O75 and NF- κ B subunits and related proteins. Target proteins for this analysis included the subunits of the most prevalent NF- κ B dimer in mammalian cells, p50 and p65, as well as I κ B α , their inhibitory interacting partner.

ICM identified two putative CU-O75 docking sites on the p50-p65-I κ B α trimer. As shown in Figure 4A, the first site is at the N terminus of I κ B α and the second at the interface between the I κ B α C terminus and the NF- κ B dimer. Given the established contribution of I κ B α 's C-terminus to the p50-p65-I κ B α trimer's stability, we hypothesized that NQBS-related compounds may stabilize this trimeric interaction, thus preventing release and nuclear translocation of the dimer. To prove the direct interaction between NQBS and I κ B α , we used the cellular thermal shift assay (CETSA), a recently developed assay to detect small-compound binding to proteins in whole-cell lysates, based on increased thermal stability of the target protein following direct small-compound protein interaction (Molina et al., 2013; Almqvist et al., 2016). Figure 4B shows the effect of the increasing temperatures on I κ B α stability in OCI-Ly10 model treated with CU-O42 and CU-O75 compared to untreated cells. A temperature of 50.1°C

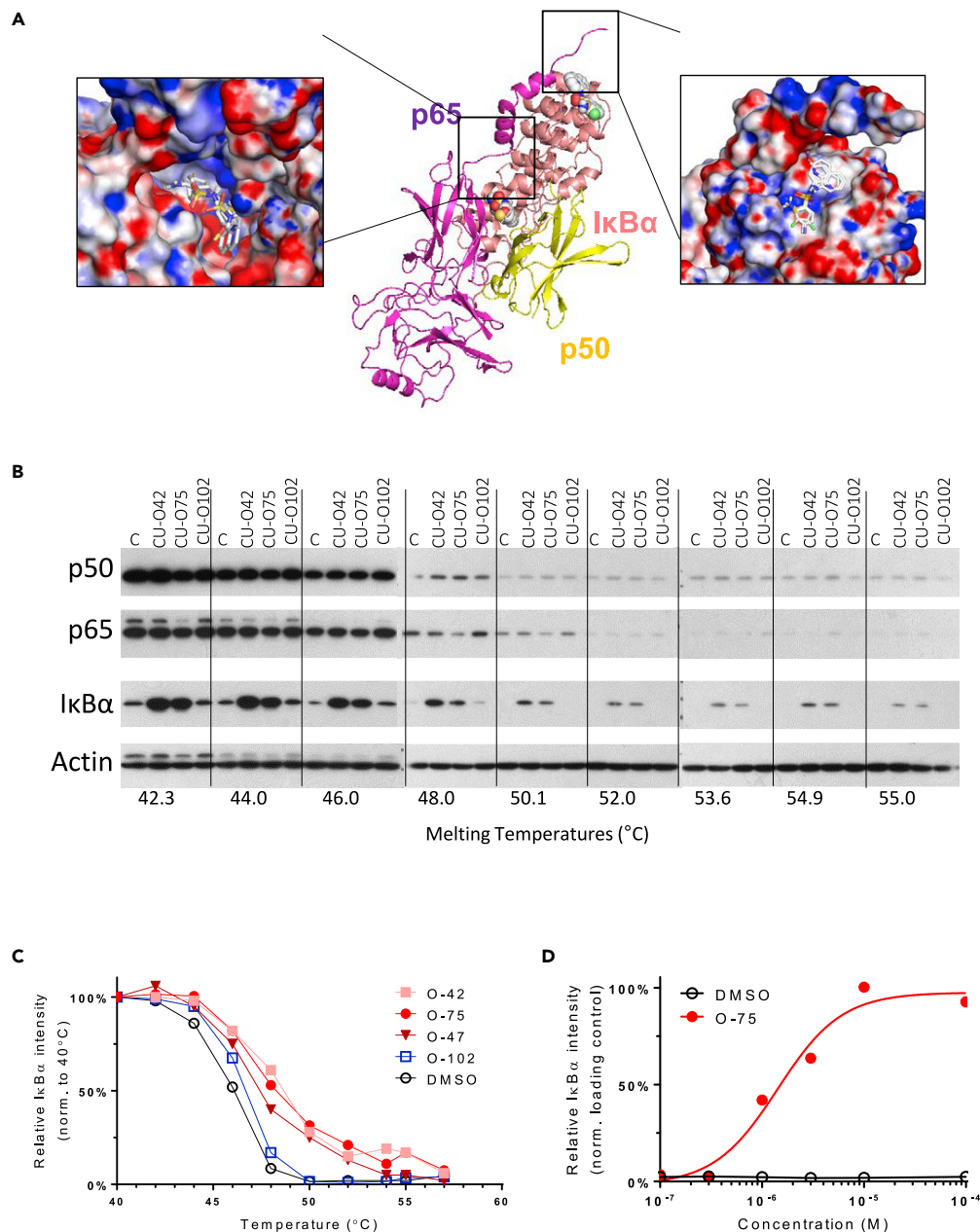


Figure 4. NQBS mechanism of action

(A) Internal Coordinate Mechanics (ICM) software analysis of potential binding sites between CU-O75 and NF- κ B subunits. ICM identified two putative docking sites of CU-O75 on the p50-p65-I κ B α trimer. First docking site is at the N terminus of I κ B α and the second at the interface of C terminus of the I κ B α with the p50-p65 dimer
 (B) Whole cellular thermal shift assay (CETSA) for I κ B α stability in OCI-Ly10 model treated with CU-O42 and CU-O75. While the temperature of 50.1°C led to full denaturation of I κ B α in the control sample and in the sample treated with inactive CU-O102 compound, I κ B α bands were readily detectable in samples treated with CU-O42 and CU-O75 at same temperatures
 (C) Thermal shift of 2.5–3.0°C for I κ B α protein mediated by CU-O42 and CU-O75 treatment of OCI-Ly10 cells
 (D) Isothermal increase in the relative I κ B α intensity observed in CU-O75-treated OCI-Ly10 cells compared to vehicle control.

led to full denaturation of I κ B α in the control sample. A similar effect was observed when OCI-Ly10 cells were incubated with the inactive CU-O102 compound. Incubation with CU-O42 and CU-O75 led to significant increase in total I κ B α at 50.1°C, consistent with increased, NQBS binding-mediated stability of the protein. Indeed, I κ B α bands were easily detectable in samples collected at up to 55°C, translating into a thermal shift of 2.5–3.0°C

(Figure 4C). Isothermal increase in the relative intensity observed in the CU-O75-treated sample compared to the vehicle control is shown in Figure 4D. This effect was not affected by translation inhibition as shown in Figure S4C. Despite the addition of cycloheximide to OCI-Ly10 cells, there was a significant increase in I κ B α levels following 3- and 6-h treatments with NQBS (CU-O75 5 μ M), compared to dimethyl sulfoxide (DMSO)-treated cells at the same time intervals. Taken together, these data suggest that NQBS compounds inhibit NF- κ B activity by stabilizing I κ B α protein complexes, rather than by preventing I κ B α degradation, thus increasing NF- κ B sequestration in the cytoplasm.

Finally, we performed RNA sequencing from CU-O75-treated OCI-Ly10 cells and analyzed the changes in gene expression compared to the vehicle-treated controls. Of the total of 288 genes found to be significantly downregulated by CU-O75, 155 (54%) were NF- κ B transcriptional targets (Figure 5A). Gene set enrichment analysis (GSEA) confirmed the observed downregulation of NF- κ B-regulated genes following 12 h treatment with CU-O75 ($p = 0.045$, Figure 5B). We next used DeMAND (Woo Hoon et al., 2015), a proteome-wide algorithm, to elucidate the mechanism of action of small-molecule compounds, based on changes in mRNA expression. DeMAND integrates the change in dependency between each protein and its network-connected targets or interactors, in a time- and concentration-dependent series of small molecule perturbations, to identify the most directly affected proteins. In NQBS-treated OCI-Ly10 cells (IC20 of CU-O75 at 24 h), DeMAND analysis identified I κ B α as a statistically significant candidate target of CU-O75 ($p = 0.003$), ranked in the top 100 proteins modified (Figure 5C).

Efficacy in In Vivo Models

To explore the anti-lymphoma effect of NQBS-related compounds *in vivo*, we chose 2 mouse lymphoma models. Figure 6A represents a double transgenic, CD19CherryLuciferase and λ -MYC mouse model that spontaneously develops aggressive B-cell lymphomas (Scotto et al., 2012). Once lymphoma development was demonstrable by luminescence analysis, we treated the animals ($n = 3$) with 4 daily intraperitoneal (i.p.) injections with CU-O42 at 10 mg/kg. CU-O42 rapidly reduced the luminescence signal measured in all regions of interest as shown graphically in Figure 6B. This effect was brief, and lymphomas grew rapidly following cessation of CU-O42 treatment.

Next, we used two DLBCL SCID (severe combined immunodeficiency) beige xenograft models engrafting OCI-Ly1 (GCB DLBCL) or HBL-1 (ABC DLBCL). Since OCI-Ly10 does not form xenografts in SCID beige mice, we used HBL-1, another ABC cell line that forms xenografts. In this cell line, NQBS were able to prevent NF- κ B translocation to the nucleus and cause lymphoma cell death similarly to OCI-Ly10. We treated both groups of mice ($n = 10$ for each cell line) with 10 mg/kg of CU-O42 for four consecutive days, administered i.p. on days 1 and 7. As shown in Figure 6C, CU-O42 was able to significantly inhibit lymphoma growth in mice with both ABC and GCB DLBCL xenografts compared to the DMSO-treated controls ($n = 10$ for each cell line). Interestingly, however, and potentially in accordance with the cell of origin hypothesis of our lymphoma xenografts, survival advantage was observed only in mice with HBL-1 lymphomas, an ABC DLBCL-derived line (Figure 6D).

Figure S5A shows that single i.p. and oral administration of CU-O75 achieved therapeutic plasma concentrations in mice that were equivalent to the concentrations in *in vitro* experiments observed to have biologic effect. I.p. administration of CU-O42 reached plasma levels that were higher than IC50 (631 ng/mL). Additionally, mice treated with CU-O42 did not exhibit significant toxicity when observed for weight loss (Figure S5B) or myelosuppression (Figure S5C). All the animals from the xenograft experiment were sacrificed when the lymphomas surpassed a volume of 2000 mm³, and none was sacrificed due to observed toxicity of CU-O42.

DISCUSSION

DLBCL is the most common aggressive lymphoma worldwide (Teras et al. 2016). While standard treatment with combination of immunotherapy and chemotherapy can achieve long-term remissions in a significant number of patients, approximately 40% of patients will eventually relapse (Coiffier et al., 2002). Mounting evidence suggests that morphologically identical disease, such as DLBCL, has a variety of genetic subtypes characterized by specific genetic lesions and oncogenic overexpression (Pasqualucci, 2013; Chapuy et al., 2018; Schmitz et al., 2018). It is, therefore, of utmost necessity to continue the search for novel treatment options for patients with DLBCL, with specific precision-medicine-based approaches, targeting drivers behind each of the lymphoma subtypes, such as NF- κ B perturbation. This is particularly true in the elderly population where the efficacy of salvage therapy regimens is limited by its toxicity.

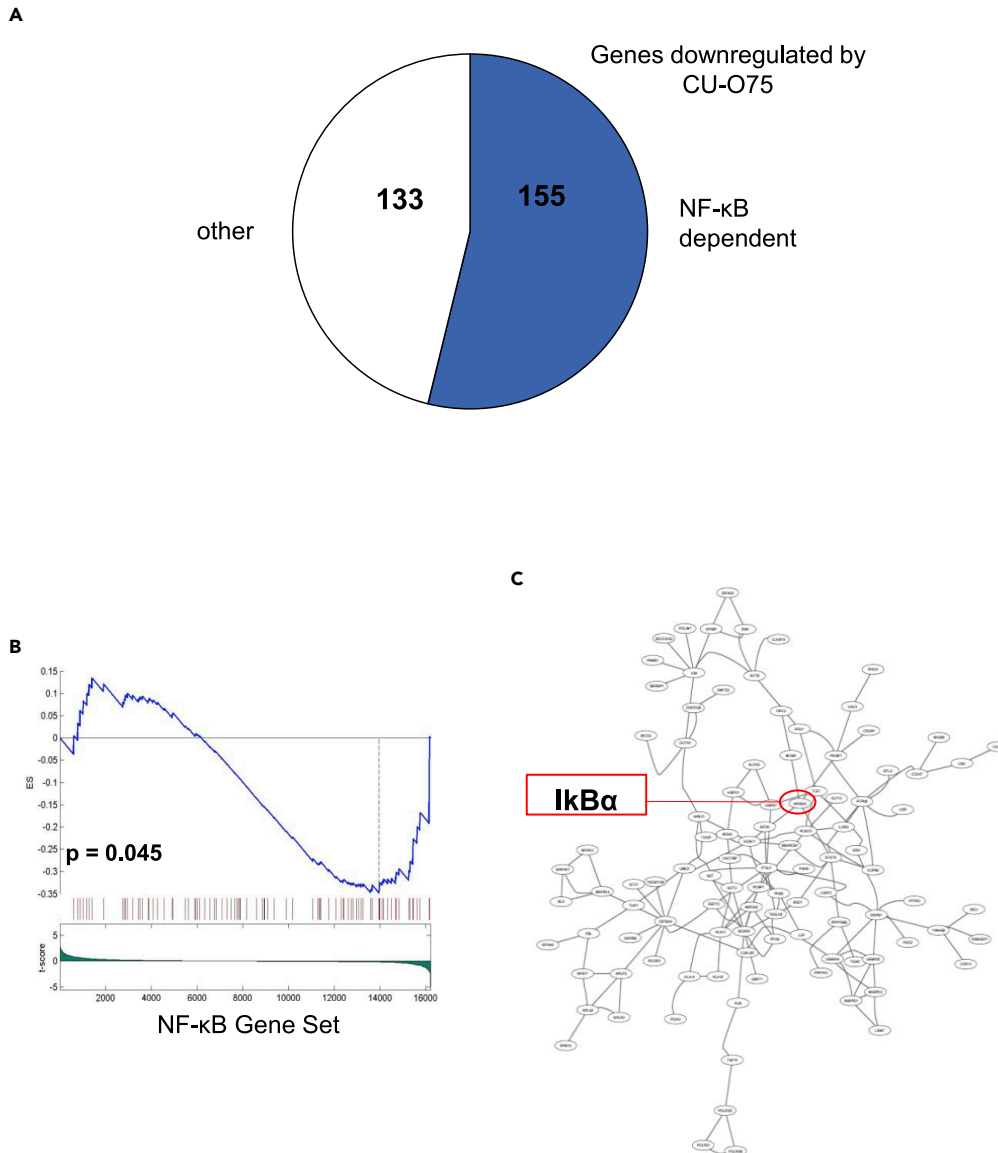


Figure 5. Gene expression changes following treatment with NQBS

(A) RNA sequencing from CU-O75-treated OCI-Ly10 demonstrates that of the total of 288 genes found to be significantly downregulated by CU-O75, 155 (54%) were NF-κB dependent

(B) Gene set enrichment analysis (GSEA) confirms downregulation of NF-κB controlled genes upon 12h treatment with CU-O75 (IC20) in OCI-Ly10

(C) DeMAND algorithm identifies IκBα as one of the top potential target proteins for CU-O75 (IC20).

We are currently witnessing unprecedented developments in immunotherapeutic treatments for hematologic malignancies. Specifically, two recent approvals of CAR T-cell-based treatment options for patients with DLBCL include axicabtagene ciloleucel and tisagenlecleucel (Neelapu et al., 2017; Schuster et al., 2019). Additionally, PD1/PDL1 inhibitors have shown efficacy in DLBCL as well (Lesokhin et al., 2016). These are, however, treatments with significant side effects, particularly in the case of CAR T cells where cytokine release syndrome and neurotoxicity are common. Furthermore, the CAR T-based treatment approach is frequently used with the understanding that they are bridging therapies to allogeneic stem cell transplants which is itself treatment burdened by significant toxicities and transplant-related mortalities.

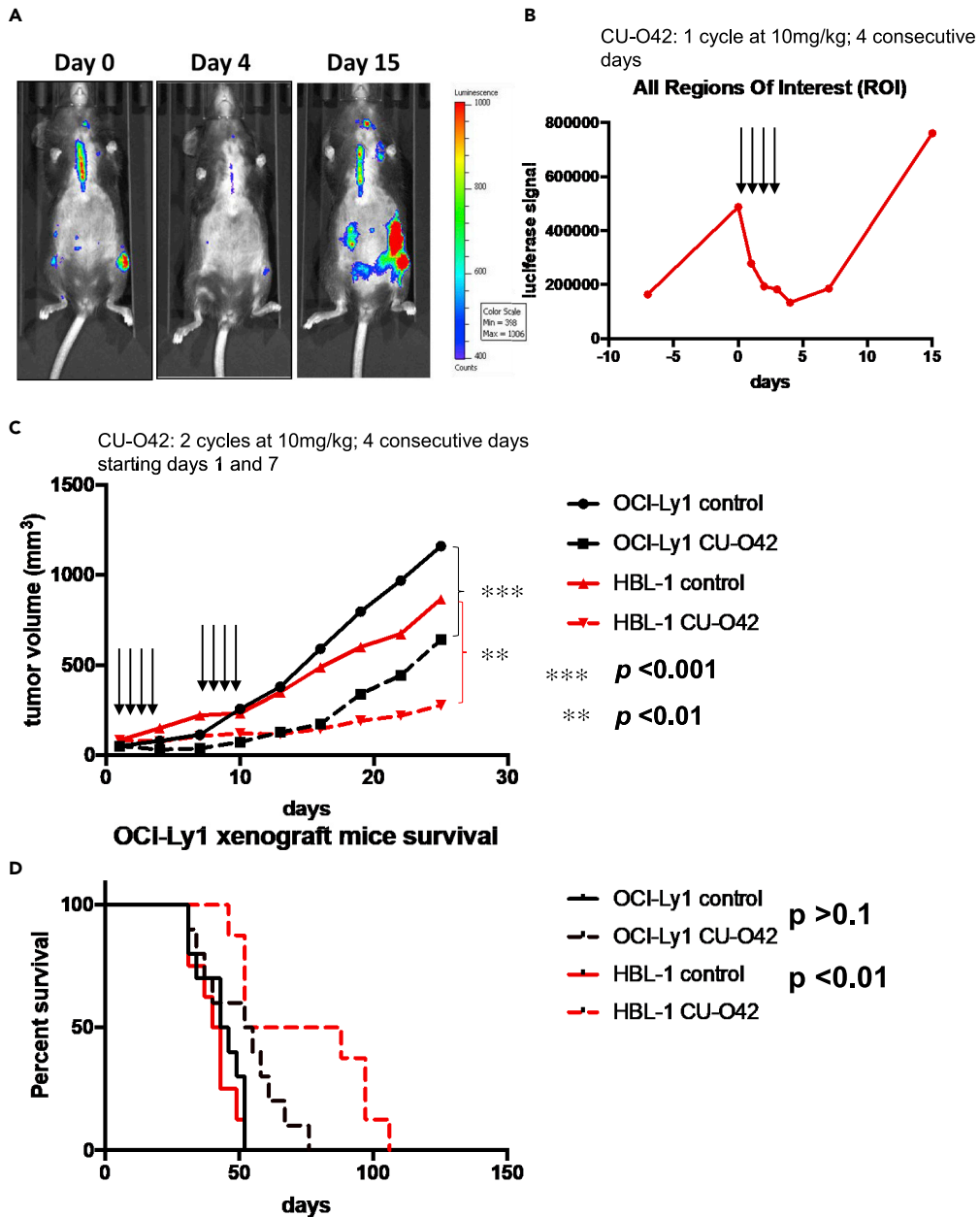


Figure 6. NQBS efficacy *in vivo*

(A) CU-O42 inhibits lymphoma growth in a double transgenic, CD19CherryLuciferase, and λ -MYC mouse model that spontaneously develops aggressive B-cell lymphomas; data for the representative animal shown.

(B) Graphic representation of CU-O42 tumor growth inhibition in double transgenic, CD19CherryLuciferase, and λ -MYC mouse model; data for the representative animal shown.

(C) DLBCL SCID (severe combined immunodeficiency) beige xenograft models with OCI-Ly1 (GC DLBCL) or HBL-1 (ABC DLBCL) demonstrating efficacy of CU-O42 in tumor growth inhibition (n = 10 for each of the treated groups)

(D) CU-O42-mediated tumor growth inhibition translated to statistically significant survival benefit in ABC DLBCL xenograft.

Given the advanced age of patients with DLBCL at diagnosis, a significant proportion may not be eligible for more aggressive immunotherapies such as CAR-T or stem cell transplants. Therefore, the development of additional therapeutic options with easy administration schedules and low-toxicity profiles, such as NQBS-related compounds, can satisfy the unmet need facing this large and growing DLBCL patient

population (Teras et al., 2016; Coiffier et al., 2002). Some of them have already shown therapeutic potential as is the example of lenalidomide and rituximab in DLBCL (Wang et al., 2013).

In this manuscript, we focus on the preclinical development of a therapeutic approach, targeting one of the most important oncogenic pathways in DLBCL – NF- κ B. NF- κ B is responsible for uncontrolled division of DLBCL cells through activating mutations downstream of the BCR, CD40L/CD40, and TLR/IL1R pathways. These include CD79A and B, CARD11, MYD88, and A20 alterations, which result in constitutive activation of NF- κ B (Davis et al., 2010). These genetic events lead to particularly adverse outcomes in patients with DLBCL whose disease carries the characteristics of activated B-cell type disease (Alizadeh et al., 2000). Multiple pro-inflammatory pathways converge to act through NF- κ B as well, which suggests its selective inhibition may play a therapeutic role in a spectrum of non-malignant conditions, such as autoimmune diseases, including rheumatoid arthritis, inflammatory bowel disease, and psoriasis.

We have shown that NOBS-related compounds, in line with the high-throughput screening platform used for their identification, potently and rapidly inhibited NF- κ B translocation to the nucleus of DLBCL cells. This effect was observed in multiple cell lines of both GCB and ABC origin and shown in multiple assays analyzing NF- κ B subunit localization in the nucleus and its binding to DNA.

Mechanistically, these compounds act by directly binding to I κ B α , increasing the cellular stability of the protein, as shown in our CETSA and cycloheximide pulse-chase assays. In turn, increased I κ B α stability resulted in presumed greater binding to the p65/p50 dimer and sequestration of the complex to the cytoplasm of lymphoma cells. Consequently, the observed effect resulted in significant decrease in RNA expression of NF- κ B-controlled target genes. Additionally, DeMAND analysis identified I κ B α as a leading potential target of NOBS-related compounds as determined from the unique gene signature generated from lymphoma cells exposed to the drugs.

Finally, NOBS-related compounds potently inhibited lymphoma growth without significant toxicities observed in two *in vivo* models of DLBCL. Interestingly, and potentially in accordance with the cell of origin hypothesis of DLBCL, survival advantage was observed only in animals with ABC xenografts treated with NOBS, while NOBS-related compounds inhibited tumor growth of both GCB and ABC xenografts. It is important to note here that the number of animals used for this experiment ($n = 10$ for each group) is limited and that a larger number of animals could make the difference in survival of treated vs. untreated mice with OCI-Ly1 xenografts statistically significant. It is also noteworthy that while HBL-1 cell line engrafts sooner in experimental animals, eventually OCI-Ly1 overgrows HBL-1, so the lack of NOBS efficacy in GCB cell line with regards to overall survival benefit could be biased by the speed of cell line growth.

In conclusion, we present strong evidence that NOBS-related compounds potently inhibit NF- κ B activity and translocation in preclinical models of DLBCL. *In vivo* efficacy and toxicity data provide encouraging evidence to support further drug development. Additional preclinical tests are being pursued to determine the suitability of these compounds for potential early phase clinical trials.

Limitations of the Study

These experiments in this manuscript are all performed in preclinical models of DLBCL, and further studies are needed to determine if NOBSs confer same mechanism of action that would be clinically meaningful. Main experiments in this study are performed using American Type Culture Collection (ATCC) -verified cell line models of DLBCL. Further work is need, particularly with primary DLBCL samples to confirm the findings reported.

Resource Availability

Lead Contact

Matko Kalac – matko.kalac@mssm.edu.

Materials Availability

Compounds reported in this study are protected by the US patent number 9,896,420.

Data and Code Availability

Microarray data are available in National Center for Biotechnology Information Gene Expression Omnibus database (accession number GSE161677).

METHODS

All methods can be found in the accompanying [Transparent Methods supplemental file](#).

SUPPLEMENTAL INFORMATION

Supplemental Information can be found online at <https://doi.org/10.1016/j.isci.2020.101884>.

ACKNOWLEDGMENTS

Work presented in this publication was partly sponsored by the American Society of Clinical Oncology's Conquer Cancer Foundation through its Young Investigator Award, by the National Center for Advancing Translational Sciences, National Institutes of Health, through Grant Number TL1TR001875 to MK, and by the Center for Target Discovery and Development U01 CA217858 to AC, as well as by the S10 OD01235 and S10 OD021764 instrumentation grants to A.C. Work presented in this publication was partly sponsored by the National Institutes of Health through its S10 instrumentation program (grant ID 1S10OD018121) to D.W.L.

AUTHOR CONTRIBUTIONS

M.K. designed and performed the experiments and wrote the manuscript, M.M. designed and performed the experiments and wrote the manuscript, A.R. synthesized the compounds and contributed to manuscript preparation, S.D. synthesized the compounds and contributed to manuscript preparation, L.S. designed and performed the experiments and contributed to manuscript preparation, M.M. designed and performed the experiments, M.B. and A.C. contributed in GSEA and DeMAND analysis, D.W.L. designed the experiments and contributed to the synthesis of the compounds, and O.A.O. designed the experiments and wrote the manuscript.

DECLARATION OF INTERESTS

A.C. is a founder, equity holder, consultant, and director of DarwinHealth Inc., a company that has licensed some of the algorithms used in this manuscript from Columbia University. Columbia University is also an equity holder in DarwinHealth Inc. N-quinolin-benzensulfonamides and related compounds' structures are submitted to the US Patent Office – US patent number 9,896,420. All remaining authors declare no conflicting interests.

Received: July 1, 2020

Revised: September 28, 2020

Accepted: November 25, 2020

Published: December 18, 2020

REFERENCES

- Alizadeh, A.A., Eisen, M.B., Davis, R.E., Ma, C., Lossos, I.S., Rosenwald, A., Boldrick, J.C., Sabet, H., Tran, T., Yu, X., et al. (2000). Distinct types of diffuse large B-cell lymphoma identified by gene expression profiling. *Nature* 403, 503–511.
- Almqvist, H., Axelsson, H., Jafari, R., Dan, C., Mateus, A., Haraldsson, M., Larsson, A., Martinez Molina, D., Artursson, P., Lundbäck, T., and Nordlund, P. (2016). CETSA screening identifies known and novel thymidylate synthase inhibitors and slow intracellular activation of 5-fluorouracil. *Nat. Commun.* 7, 11040.
- Baud, V., and Karin, M. (2009). Is NF- κ B a good target for cancer therapy? Hopes and pitfalls. *Nat. Rev. Drug Discov.* 8, 33–40.
- Brasseres, D.S., and Baldwin, A.S. (2006). Nuclear factor- κ B and inhibitor of κ B kinase pathways in oncogenic initiation and progression. *Oncogene* 25, 6817–6830.
- Chapuy, B., Stewart, C., Dunford, A.J., Kim, J., Kamburov, A., Redd, R.A., Lawrence, M.S., Roemer, M.G.M., Li, A.J., Ziepert, M., et al. (2018). Molecular subtypes of diffuse large B cell lymphoma are associated with distinct pathogenic mechanisms and outcomes. *Nat. Med.* 24, 679–690.
- Claudio, E., Brown, K., Park, S., Wang, H., and Siebenlist, U. (2002). BAFF-induced NEMO-independent processing of NF- κ B2 in maturing B cells. *Nat. Immunol.* 3, 958–965.
- Coiffier, B., Lepage, E., Briere, J., Herbrecht, R., Tilly, H., Bouabdallah, R., Morel, P., Van Den Neste, E., Salles, G., Gaulard, P., et al. (2002). CHOP chemotherapy plus rituximab compared with CHOP alone in elderly patients with diffuse large-B-cell lymphoma. *N. Engl. J. Med.* 346, 235–242.
- Coope, H.J., Atkinson, P.G., Huhse, B., Belich, M., Janzen, J., Holman, M.J., Klaus, G.G., Johnston, L.H., and Ley, S.C. (2002). CD40 regulates the processing of NF- κ B2 p100 to p52. *EMBO J.* 21, 5375–5385.
- Davis, R.E., Ngo, V.N., Lenz, G., Tolar, P., Young, R.M., Romesser, P.B., Kohlhammer, H., Lamy, L., Zhao, H., Yang, Y., et al. (2010). Chronic active B-

cell-receptor signalling in diffuse large B-cell lymphoma. *Nature* 463, 88–92.

Deng, C., Lipstein, M., Rodriguez, R., Serrano, X.O., McIntosh, C., Tsai, W.Y., Wasmuth, A.S., Jaken, S., and O'Connor, O.A. (2015). The novel IKK2 inhibitor LY2409881 potentially synergizes with histone deacetylase inhibitors in preclinical models of lymphoma through the downregulation of NF- κ B. *Clin. Cancer Res.* 21, 134–145.

Dejardin, E., Droin, N.M., Delhase, M., Haas, E., Cao, Y., Makris, C., Li, Z.W., Karin, M., Ware, C.F., and Green, D.R. (2002). The lymphotoxin-beta receptor induces different patterns of gene expression via two NF-kappaB pathways. *Immunity* 17, 525–535.

Derudder, E., Dejardin, E., Pritchard, L.L., Green, D.R., Komer, M., and Baud, V. (2003). RelB/p50 dimers are differentially regulated by tumor necrosis factor- α and lymphotoxin- β receptor activation. *J. Biol. Chem.* 278, 23278–23284.

Dutta, J., Fan, Y., Gupta, N., Fan, G., and Gelinas, C. (2006). Current insights into the regulation of programmed cell death by NF- κ B. *Oncogene* 25, 6800–6816.

Ghosh, S., and Baltimore, D. (1990). Activation in vitro on NF- κ B by its inhibitor I κ B. *Nature* 344, 679–682.

Ghosh, S., May, M.J., and Kopp, E.B. (1998). NF- κ B and Rel proteins: evolutionary conserved mediators of immune responses. *Annu. Rev. Immunol.* 16, 225–260.

Ghosh, S., and Karin, M. (2002). Missing pieces in NF- κ B puzzle. *Cell* 109, S81–S96.

Gilmore, T.D., and Herscovitch, M. (2006). Inhibitors of NF- κ B signaling:785 and counting. *Oncogene* 25, 6887–6899.

Gisselbrecht, C., Glass, B., Mounier, N., Singh Gill, D., Linch, D.C., Trneny, M., Bosly, A., Ketterer, N., Shpilberg, O., Hagberg, H., et al. (2010). Salvage regimens with autologous transplantation for relapsed large B-cell lymphoma in the rituximab era. *J. Clin. Oncol.* 28, 4184–4190.

Herndon, T.M., Deisseroth, A., Kaminskas, E., Kane, R.C., Koti, K.M., Rothmann, M.D., Habtemariam, B., Bullock, J., Bray, J.D., Hawes, J., et al. (2013). US food and drug administration approval: carfilzomib for the treatment of multiple myeloma. *Clin. Cancer Res.* 19, 4559–4563.

Herrington, F.D., Carmody, R.J., and Goodyear, C.S. (2015). Modulation of NF- κ B signaling as a therapeutic target in autoimmunity. *J. Biomol. Screen* 21, 223–242.

Kane, R.C., Bross, P.F., Farrell, A.T., and Pazdur, R. (2003). Velcade: US FDA approval for the treatment of multiple myeloma progressing on prior therapy. *Oncologist* 8, 508–513.

Karin, M. (2006). Nuclear factor- κ B in cancer development and progression. *Nature* 441, 431–436.

Kato, M., Sanada, M., Kato, I., Sato, Y., Takita, J., Takeuchi, K., Niwa, A., Chen, Y., Nakazaki, K.,

Nomoto, J., et al. (2009). Frequent inactivation of A20 in B-cell lymphomas. *Nature* 459, 712–716.

Lenz, G., Davis, R.E., Ngo, V.N., Lam, L., George, T.C., Wright, G.W., Dave, S.S., Zhao, H., Xu, W., Rosenwald, A., et al. (2008). Oncogenic CARD11 mutations in human diffuse large B-cell lymphoma. *Science* 319, 1676–1679.

Lesokhin, A.M., Ansell, S.M., Armand, P., Scott, E.C., Halwani, A., Gutierrez, M., Millenson, M.M., Cohen, A.D., Schuster, S.J., Lebovic, D., et al. (2016). Nivolumab in patients with relapsed or refractory hemaologic malignancy: preliminary results of a phase Ib study. *J. Clin. Oncol.* 34, 2698–2704.

Luo, J.L., Kamata, H., and Karin, M. (2005). The anti death machinery in IKK/NF- κ B signaling. *J. Clin. Immunol.* 25, 541–550.

Ma, J., Xing, W., Coffey, G., Dresser, K., Lu, K., Guo, A., Raca, G., Pandey, A., Conley, P., Yu, H., and Wang, Y.L. (2015). Cerdulatinib, a novel dual SYK/JAK kinase inhibitor, has broad anti-tumor activity in both ABC and GCB types of diffuse large B cell lymphoma. *Oncotarget* 6, 43881–43896.

Molina, D.M., Jafari, R., Ignatushchenko, M., Seki, T., Larsson, E.A., Dan, C., Sreekumar, L., Cao, Y., and Nordlund, P. (2013). Monitoring drug target engagement in cells and tissues using the cellular thermal shift assay. *Science* 6141, 84–87.

Neelapu, S.S., Locke, F.L., Bartlett, N.L., Lekakis, L.J., Miklos, D.B., Jacobson, C.A., Braunschweig, I., Oluwole, O.O., Siddiqi, T., Lin, Y., et al. (2017). Axicabtagene ciloleucel CAR T-cell therapy in refractory large B-cell lymphoma. *N. Eng. J. Med.* 377, 2531–2544.

Ngo, V.N., Young, R.M., Schmitz, R., Jhavar, S., Xiao, W., Lim, K.H., Kohlhammer, H., Xu, W., Yang, Y., Zhao, H., et al. (2010). Oncogenically active MYD88 mutations in human lymphoma. *Nature* 470, 115–119.

Nowakowski, G.S., LaPlant, B., Macon, W.R., Reeder, C.B., Foran, J.M., Nelson, G.D., Thompson, C.A., Rivera, C.E., Inwards, D.J., Micallef, I.N., et al. (2015). Lenalidomide combined with R-CHOP overcomes negative prognostic impact of non-germinal center B-cell phenotype in newly diagnosed diffuse large B-Cell lymphoma: a phase II study. *J. Clin. Oncol.* 33, 251–257.

Oeckinghouse, A., Hayden, M.S., and Ghosh, S. (2011). Crosstalk in NF- κ B signaling pathways. *Nat. Immunol.* 12, 695–708.

Pasqualucci, L. (2013). The genetic basis of diffuse large B-cell lymphoma. *Curr. Opin. Hematol.* 20, 336–344.

Schmitz, R., Wright, G.W., Huang, D.W., Johnson, C.A., Phelan, J.D., Wang, J.Q., Roulland, S., Kasbekar, M., Young, R.M., Shaffer, A.L., et al. (2018). Genetics and pathogenesis of diffuse large B-cell lymphoma. *N. Eng. J. Med.* 378, 1396–1407.

Schuster, S.J., Bishop, M.R., Tam, C.S., Waller, E.K., Borchmann, P., McGuirk, J.P., Jäger, U., Jaglowski, S., Andreadis, C., Westin, J.R., et al. (2019). Tisagenlecleucel in adult relapsed or refractory diffuse large B-cell lymphoma. *N. Engl. J. Med.* 380, 45–56.

Scotto, L., Kruihof-de Julio, M., Paoluzzi, L., Kalac, M., Marchi, E., Buitrago, J.B., Amengual, J., Shen, M.M., and O'Connor, O.A. (2012). Development and characterization of a novel CD19CherryLuciferase (CD19CL) transgenic mouse for the preclinical study of B-cell lymphomas. *Clin. Cancer Res.* 18, 3803–3811.

Shaffer, A.L., 3rd, Young, R.M., and Staudt, L.M. (2012). Pathogenesis of human B-cell lymphomas. *Annu. Rev. Immunol.* 30, 565–610.

Swerdlow, S.H., Campo, E., Harris, N.L., Jaffe, E.S., Pileri, S.A., Stein, H., Thiele, J., and Vardiman, J.W. (2008). WHO Classification of Tumours of Haematopoietic and Lymphoid Tissues (International Agency for Research on Cancer (IARC)).

Teras, L.R., DeSantis, C.E., Cerhan, J.R., Morton, L.M., Jemal, A., and Flowers, C.R. (2016). US lymphoid malignancy statistics by world Health organization subtypes. *CA Cancer J. Clin.* 66, 443–459.

Viardot, A., Goebeler, M.E., Hess, G., Neumann, S., Pfreundschuh, M., Adrian, N., Zettl, F., Libicher, M., Sayehli, C., Stieglmaier, J., et al. (2016). Phase 2 study of the bispecific T-cell engager (BiTE) antibody blinatumomab in relapsed/refractory diffuse large B-cell lymphoma. *Blood* 127, 1410–1416.

Wang, M., Fowler, N., Wagner-Bartak, N., Feng, L., Romaguera, J., Neelapu, S.S., Hagemester, F., Fanale, M., Oki, Y., Pro, B., et al. (2013). Oral lenalidomide with rituximab in relapsed or refractory diffuse large cell, follicular and transformed lymphoma: a phase II clinical trial. *Leukemia* 27, 1902–1909.

Woo, J.H., Shimoni, Y., Yang, W.S., Subramaniam, P., Iyer, A., Nicoletti, P., Rodriguez Martinez, M., López, G., Mattioli, M., Realubit, R., et al. (2015). Elucidating compound mechanism of action by network perturbation analysis. *Cell* 162, 441–451.

Xiao, G., Harhaj, E.W., and Sun, S.C. (2001). NF- κ B-inducing kinase regulates the processing of NF- κ B p100. *Mol. Cell* 7, 401–409.

Xie, Y., Deng, S., Thomas, C.J., Liu, Y., Zhang, Y.Q., Rinderspacher, A., Huang, W., Gong, G., Wylter, M., Cayanis, E., et al. (2008). Identification of N-(quinolin-8-yl)benzenesulfonamides as agents capable of down-regulating NF κ B activity within two separate high-throughput screens of NF κ B activation. *Bioorg. Med. Chem. Lett.* 18, 329–335.

Younes, A., Sehn, L.H., Johnson, P., Zinzani, P.L., Hong, X., Zhu, J., Patti, C., Belada, D., Samoilova, O., Suh, C., et al. (2019). Randomized phase III trial of ibrutinib and rituximab plus cyclophosphamide, doxorubicin, vincristine, and prednisone in non-germinal center B-cell diffuse large B-cell lymphoma. *J. Clin. Oncol.* 37, 1285–1295.

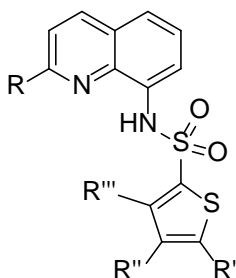
Younes, A., Thieblemont, C., Morschhauser, F., Flinn, I., Friedberg, J.W., Amorim, S., Hivert, B., Westin, J., Vermeulen, J., Bandyopadhyay, N., et al. (2014). Combination of ibrutinib with rituximab, cyclophosphamide, doxorubicin, vincristine, and prednisone (R-CHOP) for treatment-naïve patients with CD20-positive B-cell non-Hodgkin lymphoma: a non-randomised, phase 1b study. *Lancet Oncol.* 15, 1019.

Supplemental Information

***N*-quinoline-benzenesulfonamide
derivatives exert potent anti-lymphoma
effect by targeting NF- κ B**

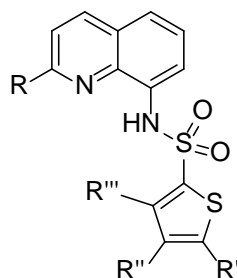
Matko Kalac, Michael Mangone, Alison Rinderspacher, Shi-Xian Deng, Luigi Scotto, Michael Markson, Mukesh Bansal, Andrea Califano, Donald W. Landry, and Owen A. O'Connor

Supplemental Table 1. Halo Substituents at the 4- and 5-positions of the Thiophene Ring. Related to Figure 1.



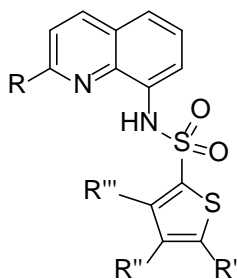
Compound #	R	R'	R''	R'''	Ly1 IC ₅₀ [μM]	Ly10 IC ₅₀ [μM]
O-4	CH ₃	Br	H	H	1.4	1.5
O-19	H	Cl	H	H	0.8	0.7
O-25	CH ₃	Cl	H	H	1.3	0.8
O-47	H	Cl	Cl	H	0.7	0.7
O-50	CH ₃	Cl	Cl	H	>10	>10
O-49	H	Br	Br	H	1.4	1.5
O-52	CH ₃	Br	Br	H	>10	>10
O-83	H	F	H	H	1.5	1.1

Supplemental Table 2. Substituents at the 4- and 5-positions of the Thiophene Ring. Related to Figure 1.



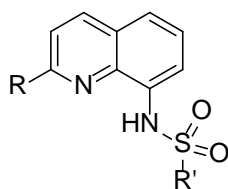
Compound #	R	R'	R''	R'''	Ly1 IC ₅₀ [μM]	Ly10 IC ₅₀ [μM]
O-48	H	Cl	NO ₂	H	>10	>10
O-51	CH ₃	Cl	NO ₂	H	>10	>10
O-55	H	Cl	Br	H	0.5	0.5
O-56	CH ₃	Cl	Br	H	>10	>10

Supplemental Table 3. Alkyl and Aryl Substituents at the 3-, 4-, and 5-positions of the Thiophene Ring. Related to Figure 1.



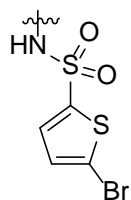
Compound #	R	R'	R''	R'''	Ly1 IC ₅₀ [μM]	Ly10 IC ₅₀ [μM]
O-61	H	Me	H	H	1.1	2.4
O-66	Me	Me	H	H	0.6	1.7
O-59	H	Et	H	H	1.4	2.6
O-64	Me	Et	H	H	1.6	3.2
O-60	H	H	H	Me	1.3	2.6
O-65	Me	H	H	Me	>10	>10
O-97	H	Ph	H	H	3.2	5.5
O-98	Me	Ph	H	H	4	27
O-87	H	H	CO ₂ H	H	>10	>10

Supplemental Table 4. Different Heterocyclic Substituents. Related to Figure 1.



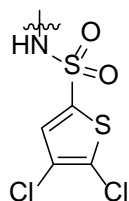
Compound #	R	R'	Ly1 IC ₅₀ [μM]	Ly10 IC ₅₀ [μM]
O-53	H		>10	>10
O-54	Me		6.3	5.4
O-90	H		>10	>10
O-57	H		1.7	3.1
O-58	Me		1.4	2.6
O-63	H		>10	>10
O-67	Me		Not tested	Not tested
O-62	H		>10	>10

Supplemental Table 5A. Different Cores. Related to Figure 1.



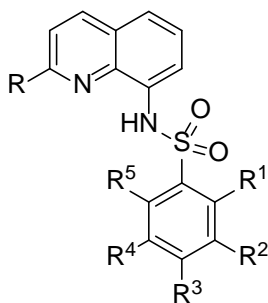
Compound #	CORE	Ly1 IC ₅₀ [μM]	Ly10 IC ₅₀ [μM]
O-84		>10	>10
O-85		6.3	5.4
O-88		>10	>10
O-89		1.7	3.1
O-91		1.4	2.6
O-94		>10	>10

Supplemental Table 5B. Different Cores.
Related to Figure 1.



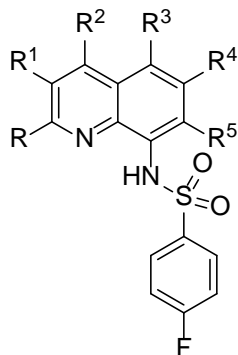
Compound #	CORE	Ly1 IC ₅₀ [μM]	Ly10 IC ₅₀ [μM]
O-92		>10	>10
O-93		>10	>10
O-103		>10	>10
O-111		NO DATA	5

Supplemental Table 6. Substituted Phenyl Groups. Related to Figure 1.



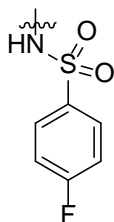
Compound #	R	R ¹	R ²	R ³	R ⁴	R ⁵	Ly1 IC ₅₀ [μM]	Ly10 IC ₅₀ [μM]
O-68	H	Br	H	H	H	H	1.5	1.2
O-69	H	H	H	Cl	H	H	0.7	0.7
O-70	H	Cl	H	H	H	H	1.1	1.2
O-71	H	H	Cl	H	H	H	1.2	1.2
O-72	H	H	Br	H	H	H	1.9	1.5
O-73	H	F	H	H	H	H	0.9	1
O-74	H	H	F	H	H	H	0.7	0.7
O-75	H	H	H	F	H	H	0.7	0.7
O-76	Me	Br	H	H	H	H	3.7	3.9
O-77	Me	H	H	Cl	H	H	1.5	1.2
O-78	Me	Cl	H	H	H	H	3.8	3
O-79	Me	H	Cl	H	H	H	1.7	1.6
O-80	Me	H	Br	H	H	H	1.2	1
O-81	Me	F	H	H	H	H	1.8	1.9
O-82	Me	H	F	H	H	H	1.5	1
O-86	Me	H	H	F	H	H	2.1	2.3
O-95	H	H	H	Br	H	H	1	1.5
O-96	Me	H	H	Br	H	H	1.4	1.8
O-99	H	H	H	NO ₂	H	H	>10	>10
O-104	H	H	OMe	OMe	H	H		>5
O-105	H	H	H	OMe	H	H		4.5
O-106	H	H	H	OCF ₃	H	H		2.5
O-107	H	H	H	OCH ₂ CO ₂ H	H	H		>5
O-110	H	H	COOH	F	H	H	2	2
O-113	H	H	H	I	H	H		2

Supplemental Table 7. Substituted Cores. Related to Figure 1.



Compound #	R	R ¹	R ²	R ³	R ⁴	R ⁵	Ly1 IC ₅₀ [μM]	Ly10 IC ₅₀ [μM]
O-109	H	H	Me	H	H	H	1.5	1.5
O-117	H	H	OMe	H	H	H	1.3	2.3
O-118	H	H	OCH ₂ CO ₂ H	OCF ₃	H	H	>10	>10

Supplemental Table 8. Different Cores. Related to Figure 1.

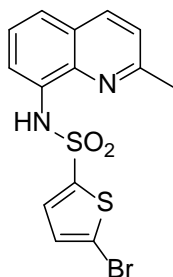


Compound #	CORE	Ly1 IC ₅₀ [μM]	Ly10 IC ₅₀ [μM]
O-102		>10	>10
O-108			>10
O-114		>10	>10
O-115		>10	>10

Supplemental Figure 1 – Spectral analysis of CU-O42, CU-O47, CU-O75 and CU-O102. Related to Figure 1B.

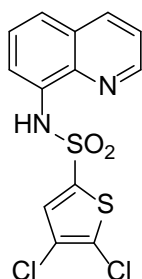
Spectral analysis - ^1H NMR and ^{13}C NMR spectra were recorded on an Agilent 400-MR 400-MHz NMR spectrometer. Chemical shifts are reported in parts per million using the residual proton or carbon signal ($(\text{CD}_3)_2\text{CO}$: δH 2.05, δc 29.84; CDCl_3 : δH 7.26, δc 77.16; and $(\text{CD}_3)_2\text{SO}$: δH 2.50, δc 39.52) as an internal reference. The apparent multiplicity (s = singlet, d = doublet, t = triplet, q = quartet, m = multiplet) and coupling constants (in Hz) are reported in that order in the parentheses after the chemical shift. Liquid chromatography and mass spectrometry were performed on a Shimadzu 2020 UFLC mass spectrometer, using a Waters Sunfire column (C18, $5\mu\text{m}$, 2.1 mm x 50 mm, a linear gradient from 5 % to 100 % B over 15 min, then 100 % B for 2 min (A = 0.1 % formic acid + H_2O , B = 0.1 % formic acid + CH_3CN), flow rate 0.2000 mL/min. High-resolution mass spectrometry was performed by Dr. Brandon Fowler at Columbia University.

CU-O42



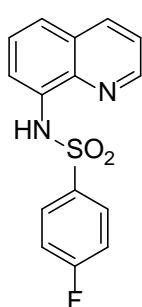
Yellow solid; Yield: 77 %; ^1H NMR (400 MHz, CDCl_3): δ 9.34 (br s, 1H), 8.01 (d, J = 8.4 Hz, 1H), 7.83 (d, J = 7.6 Hz, 1H), 7.43 (d, J = 8.0 Hz, 1H), 7.35-7.30 (m, 3H), 6.88 (d, J = 3.6 Hz, 1H), 2.70 (s, 3H), ; ^{13}C NMR (101 MHz, CDCl_3): δ 158.3, 140.8, 138.2, 136.5, 133.0, 132.7, 130.2, 126.5, 125.9, 123.2, 122.7, 120.2, 115.7, 25.3; LC-MS ($\text{M}^+\text{+H}$): 385.

CU-O47



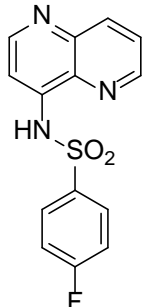
Yellow solid; Yield: 75 %; ^1H NMR (400 MHz, CDCl_3): δ 9.33 (br s, 1H), 8.79 (d, J = 2.8 Hz, 1H), 8.17 (d, J = 8.0 Hz, 1H), 7.88 (d, J = 7.2 Hz, 1H), 7.59-7.51 (m, 2H), 7.48 (dd, J = 8.4 Hz, J = 4.4 Hz, 1H), 7.39 (s, 1H), ; ^{13}C NMR (101 MHz, CDCl_3): δ 149.2, 138.8, 136.6, 133.0, 131.5, 128.5, 127.0, 124.8, 123.4, 122.4, 115.8; LC-MS ($\text{M}^+\text{+H}$): 359.

CU-O75



Clear, colorless crystals; Yield: 54 %; ^1H NMR (400 MHz, $(\text{CD}_3)_2\text{CO}$): δ 9.40 (br s, 1H), 8.84 (dd, J = 4.4 Hz, J = 1.6 Hz, 1H), 8.34 (dd, J = 8.4 Hz, J = 1.2 Hz, 1H), 8.02 (dd, J = 8.8 Hz, J = 5.2 Hz, 2H), 7.87 (d, J = 7.6 Hz, 1H), 7.66 (d, J = 8.4 Hz, 1H), 7.60-7.53 (m, 2H), 7.23 (t, J = 8.8 Hz, 2H); ^{13}C NMR (101 MHz, CDCl_3): δ 165.3 ($^1J_{\text{C-F}}$ = 255.5 Hz), 149.0, 138.7, 136.4, 135.5 ($^4J_{\text{C-F}}$ = 3.1 Hz), 133.7, 132.3, 132.2, 130.1 ($^3J_{\text{C-F}}$ = 9.9 Hz), 128.3, 126.9, 122.6, 122.2, 116.2 ($^2J_{\text{C-F}}$ = 22.8 Hz), 115.6; LC-MS ($\text{M}^+\text{+H}$): 303.

CU-O102



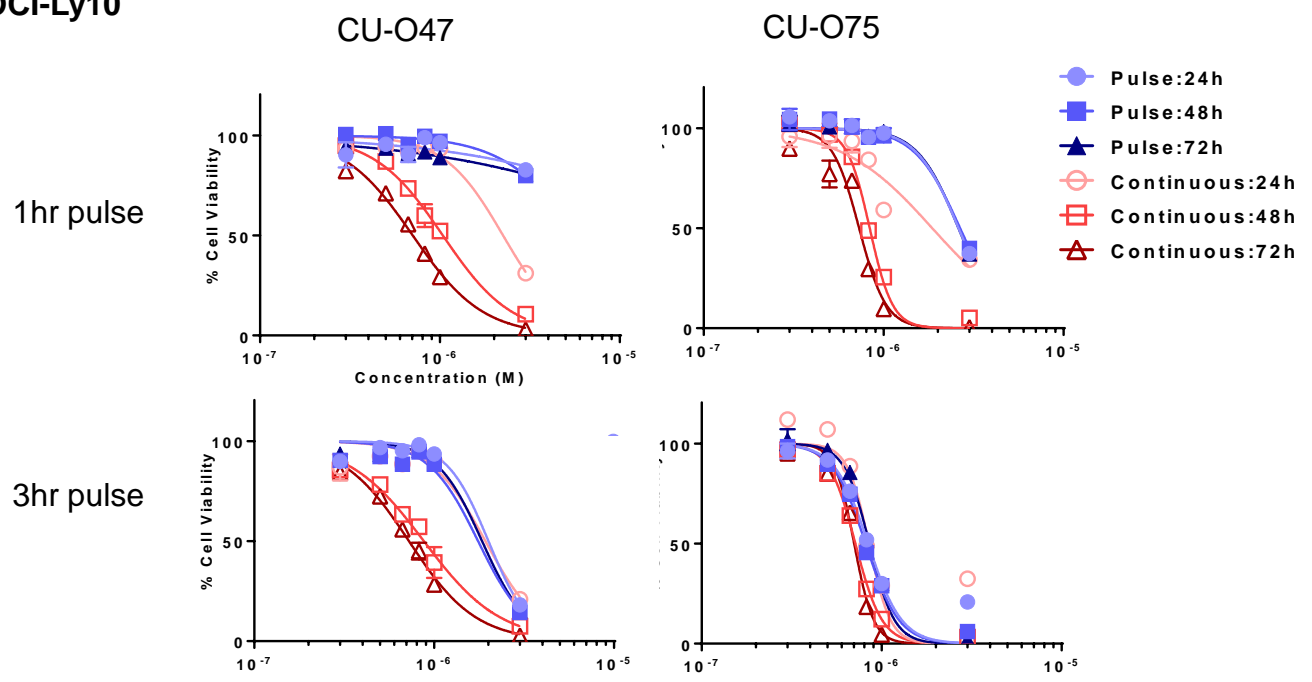
Orange-yellow solid; Yield: 44 %; ^1H NMR (400 MHz, $(\text{CD}_3)_2\text{SO}$): δ 8.88 (d, J = 3.2 Hz, 1H), 8.46 (s br, 1H), 8.22 (d, J = 8.4 Hz, 1H), 8.04 (dd, J = 8.4 Hz, J = 5.2 Hz, 2H), 7.80 (dd, J = 8.8 Hz, J = 4.4 Hz, 1H), 7.43 (d, J = 6.8 Hz, 1H), 7.38 (t, J = 8.8 Hz, 2H); ^{13}C NMR (101 MHz, $(\text{CD}_3)_2\text{SO}$): δ 164.0 ($^1J_{\text{C-F}}$ = 251.8 Hz), 149.0 (2C), 138.2, 136.2, 129.5 ($^3J_{\text{C-F}}$ = 9.1 Hz) (2C), 126.4 (2C), 116.1 ($^2J_{\text{C-F}}$ = 22.9 Hz) (2C), 107.8 (2C); LC-MS ($\text{M}^+\text{+H}$): 304; ESI + HRMS (m/z): [$\text{M}^+\text{+H}$] $^+$ calcd. for $\text{C}_{14}\text{H}_{11}\text{FN}_3\text{O}_2\text{S}$: 304.0551, Found: 304.0556.

Supplemental Figure 2 – IC50 growth inhibition values in lymphoma cell lines (DLBCL and mantle cell lymphoma) as measured by ATP luminescence based assay after incubation with NQBS for 72h. Related to Figure 2A and 2B.

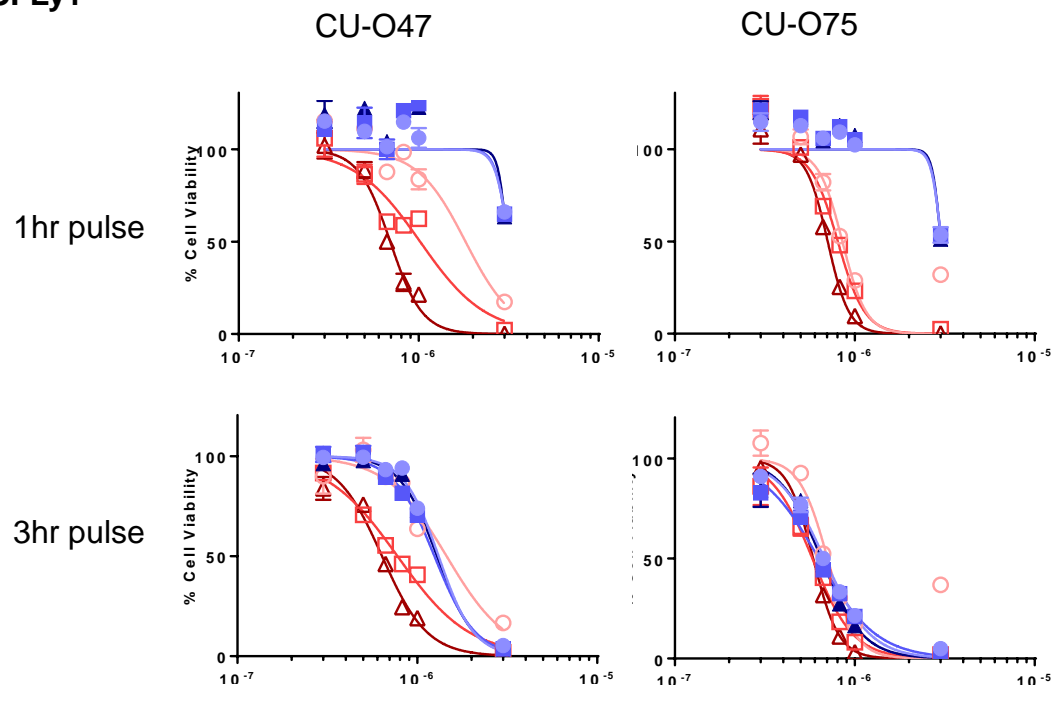
subtype	ABC DLBCL				GCB DLBCL		MCL
cell line	OCI-Ly10	SuDHL-2	HBL-1	RIVA	OCI-Ly1	SuDHL-6	HBL-2
IC ₅₀ (μM)	1.00	0.84	2.31	1.51	0.77	0.75	1.24

Supplemental Figure 3 – A pulse chase experiment analyzing cell growth inhibition in DLBCL cell lines treated with CU-O47 and CU-O-75. Related to Figure 2.

OCI-Ly10

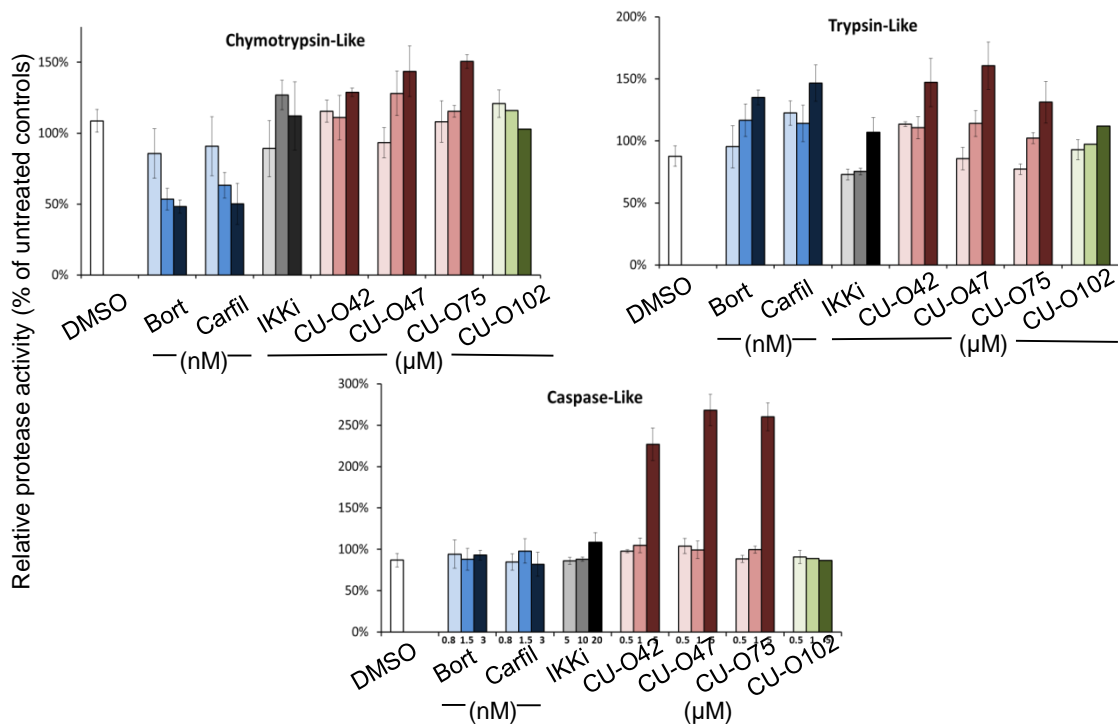


OCI-Ly1

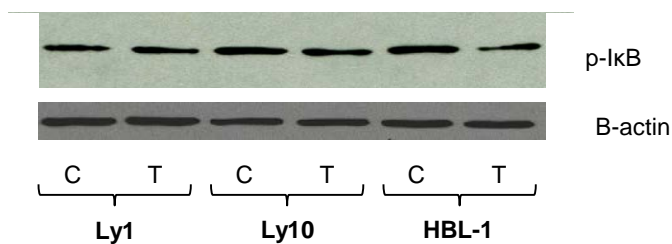


Supplemental Figure 4 – NQBS mechanism of action. Related to Figure 4.

A.



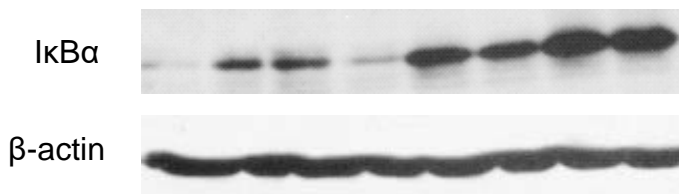
B.



C = control
T = CU-O42 (4 μM)

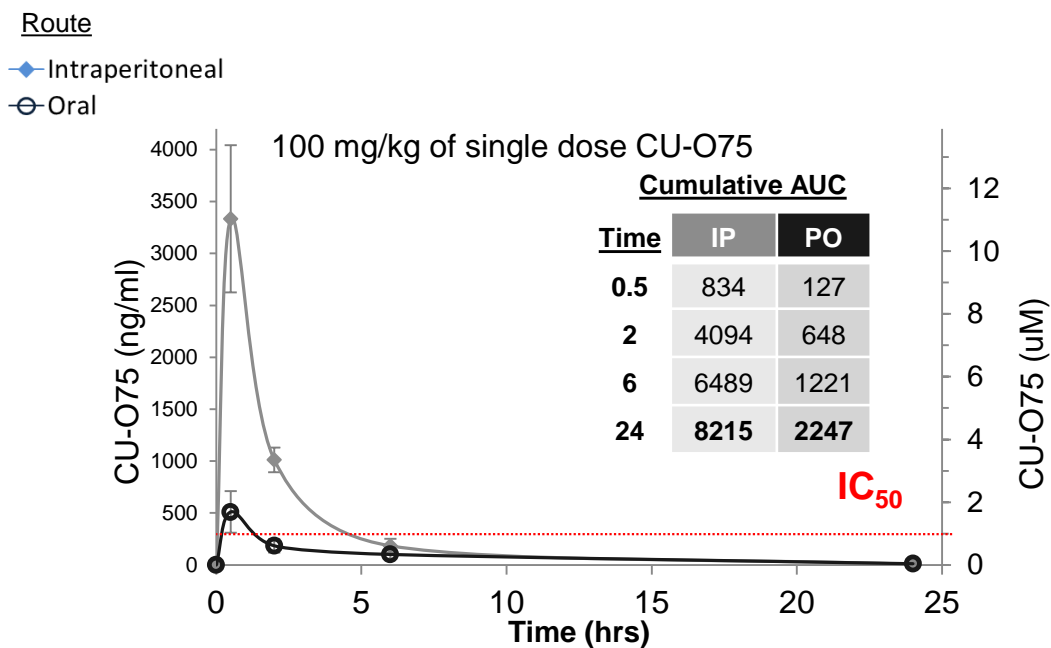
C.

Time (h)	0	3	6	0	3	6	3	6
CHX	-	+	+	+	+	+	-	-
CU-O75	-	-	-	-	+	+	+	+

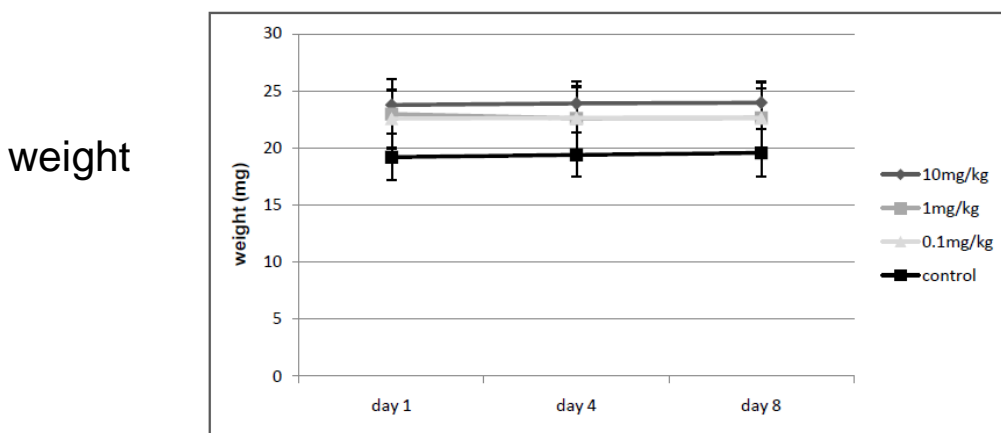


Supplemental Figure 5 – NQBS pharmacokinetics and toxicity. Related to Figure 6.

A.

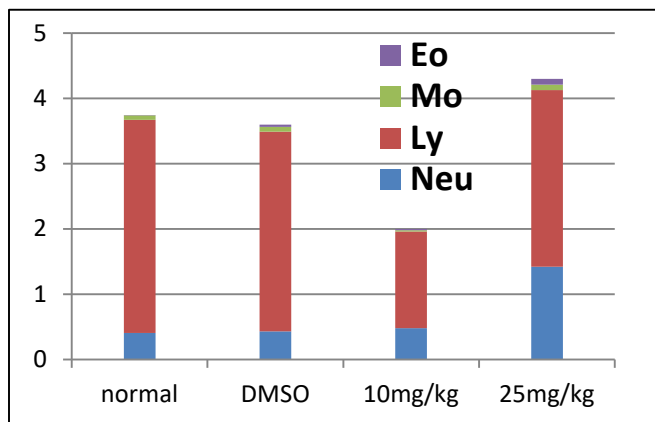


B.

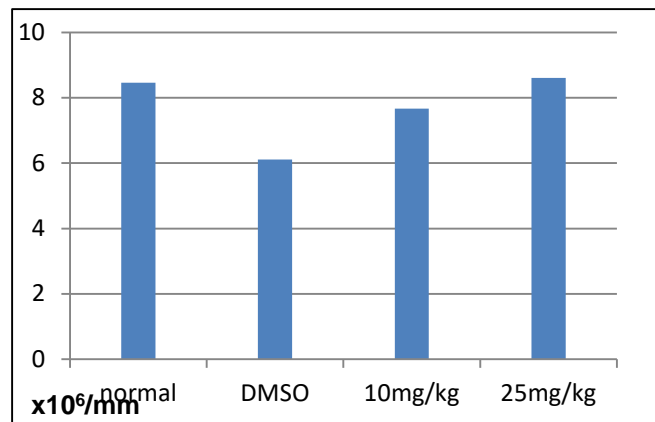


C.

WBC with differential



RBC



Transparent Methods

Cell lines. OCI-Ly1, OCI-Ly7 and Su-DHL6 are germinal center diffuse large B-cell lymphoma cell lines; OCI-Ly10, OCI-Ly3, RIVA, Su-DHL8 and Su-DHL2 are activated B-cell DLBCL lines; HBL-2 is a mantle cell lymphoma line. All the cell lines with the exception of Su-DHL6 were grown in IMDM medium with 10% fetal calf serum (FCS); Su-DHL6 was grown in RPMI medium with 10% FCS. Fresh medium was added every 2-3 days and the cells were kept at a cell concentration of $0.3\text{-}0.8 \times 10^6/\text{mL}$. Cell lines were kindly provided from Dr. Ricardo Dalla Favera's lab and German Collection of Microorganisms and Cell Cultures GmbH and were verified by the ATCC.

Materials including cell growing medium and fetal calf serum were purchased from Thermo Fisher.

Compound synthesis.

General Procedure

Conditions A: 8-Aminoquinoline (1 equiv) was stirred in a 2:1 mixture of methylene chloride and pyridine at room temperature. The respective sulfonyl chloride (1 equiv) was added. The reaction mixture was stirred overnight, then concentrated *in vacuo* and purified via column chromatography (1:1 hexanes:ethyl acetate).

Conditions B: The respective sulfonyl chloride (1 equiv) was stirred in methylene chloride at room temperature. 8-Aminoquinoline (1 equiv) was added, followed by triethylamine (3 equiv). The reaction mixture was stirred overnight, then concentrated *in vacuo* and purified via column chromatography (1:1 EtOAc:CHCl₃).

Cell viability was evaluated using the Cell-Titer-Glo Reagent (Promega) as previously reported (Kalac et al., 2011). Cells were counted and re-suspended at an approximate concentration of 3×10^5 per well in a 96-well plate and incubated at 37°C in a 5% CO₂ humidified incubator for up

to 72 hours. Subsequently, NQBS were added at concentrations from 100 nmol/L up to 20 μ mol/L to determine growth inhibition curves for all cell lines. Following incubation at 37°C in a 5% CO₂ humidified incubator, 100 μ L from each well was transferred to a 96-well opaque-walled plate; CellTiter-Glo reagent was used according to the manufacturer's instruction. The plates were allowed to incubate at room temperature for 10 minutes before recording luminescence with a Synergy HT Multi-Detection Microplate Reader (Biotek Instruments, Inc.). Each experiment was done in triplicate and repeated at least twice.

Flow cytometry. To study apoptosis, Yo-Pro-1 and propidium iodide (PI) were used (Vybrant apoptosis assay kit 4, Invitrogen, Carlsbad, CA) as previously described¹. Briefly, cells were seeded at a density of 3×10^5 /mL and incubated with NQBS for up to 72 hours. A minimum of 1×10^5 events were acquired from each sample. To quantitate apoptosis, Yo-Pro-1 and propidium iodide (PI) were used (Vybrant apoptosis assay kit #4, Invitrogen) according to the manufacturer's instruction. The fluorescence signals acquired by a FACSCalibur System were resolved by detection in the conventional FL1 and FL3 channels. Cells were considered early apoptotic if Yo-Pro-1 positive but PI negative, late apoptotic if Yo-Pro-1 and PI positive, and dead if only PI positive. Each experiment was done in triplicate and repeated at least twice.

Western blotting was performed as previously reported¹. Briefly, cells were incubated with the same concentrations of NQBS used in the apoptosis and caspase assays under normal growth conditions for up to 24 hours. Proteins from total cell lysates were resolved on 4% to 20% SDS-PAGE and transferred onto nylon membranes. Membranes were blocked in PBS, 0.05% Tween 20 containing 5% skim milk powder or BSA and were then probed overnight with specific primary antibodies. Antibodies were detected with the corresponding horseradish peroxidase-linked secondary antibodies. Blots were developed using SuperSignal West Pico chemiluminescent substrate detection reagents. The membranes were exposed to X-ray films for various time intervals. The images were captured with a GS-800 calibrated densitometer (Bio-Rad).

Antibodies were purchased from the following vendors:

1. Cell Signaling: p50 (#3035), p65 (#8242), Ku-80 (#2753), Caspase 8 (#4790), PARP (#9532), Lamin B1 (#13435), XIAP (#14334), BID (#2002), beta actin (#3700), pan ubiquitin (#3936), anti-rabbit (#7074) and anti-mouse (#7076);
2. Santa Cruz: IκBα (sc-373893).

Nuclear protein extracts were prepared using the NE-PER Nuclear and Cytoplasmic Extraction Reagents (Thermo Fisher) as per manufacturer's instructions.

Immunofluorescence was performed as follows. After incubation with NQBS for 1-12 hours, the samples were placed on the slides using the cytospin. After fixation in 10% formalin and 100% methanol, the slides were transferred to the blocking buffer (10% nonfat dry milk) and incubated with primary antibody in the humidity chamber overnight. The slides were then incubated with fluorochrome-conjugated secondary antibody for 45 minutes and mounted with 4,6-diamidino-2-phenylindole. The images were collected using Nikon Eclipse TE 2000-E inverted epifluorescent microscope, a 40×/0.60 oil objective, and a Nikon Photometrics Coolsnap HQ2 camera. The images were analyzed using NIS-Elements AR 3.2 software and Volocity 5.5.1 software. Anti-p50 (#3035), anti-Ku80 (#2753) antibodies from Cell Signaling and Cy2- and Cy3-conjugated donkey anti-rabbit IgG (Jackson ImmunoResearch) secondary antibody were used. DAPI staining was used for nuclear localization (ThermoFisher).

Electrophoretic mobility shift assay (LightShift® Chemiluminescent EMSA Kit) was purchased from Thermo Fisher and performed as per manufacturer's instructions. Cells were incubated in the same manner as for immunoblotting. Cell pellets were collected after incubation with NQBS for 3-24h. Nuclear protein extracts were prepared using the NE-PER Nuclear and Cytoplasmic Extraction Reagents (Thermo Fisher) as per manufacturer's instructions. Collected samples and controls were run on a polyacrylamide gel in 0.5X TBE and transferred onto nylon membranes.

Membranes were subsequently cross-linked at 120mJ/cm² using a commercial UV-light crosslinking instrument equipped with 254nm bulbs for 60 seconds. Membranes were then incubated in blocking buffer, washed and incubated in Substrate Equilibration Buffer and Substrate Working solution. The membranes were exposed to X-ray films for various time intervals. The images were captured with a GS-800 calibrated densitometer (Bio-Rad).

Kinome screen. We utilized KINOMEscan platform as per manufacturer's instructions (DiscoverX, Fremont, CA).

Internal Coordinate Mechanics (ICM) software was utilized as previously reported (Neves et al., 2012). We have used the following p50-p65-IkB α structure: <https://www.rcsb.org/structure/1IKN>

ICM software can be downloaded from: <https://www.molsoft.com/download.html>

Cellular thermal shift assay as previously described (Jafari et al., 2014). OCI-Ly10 cells were seeded at 4 x 10⁵/mL and incubated with NQBS for 3h. The cells were subsequently washed and re-suspended in warmed PBS and protease inhibitor at a concentration of 3 x 10⁷/mL. An aliquot (100 μ L) was transferred to PCR tubes which were placed on a thermocycler. Samples were heated at temperatures from 40-55 °C at the gradient program (3 minutes heated gradient, 3 minutes 25 °C). Samples were snap frozen and places in -80 °C overnight. This was followed by cell lysis and the separation of cell debris and aggregates from the soluble protein fraction. Immunoblotting was used to analyze the results.

Generation of Gene Expression Profiles and DeMAND analysis was performed as previously described (Wee et al., 2015). We have used OCI-Ly10 samples treated with DMSO; IC20 value of CU-O75; and 1/10 of the IC20 value of CU-O75 at 12 and 24h. Download of DeMAND software available at: <http://califano.c2b2.columbia.edu/demand>

GSEA was performed as previously described (Subramanian et al., 2005). OCI-Ly10 samples used for GSEA were treated with DMSO; IC20 value of CU-O75; and 1/10 of the IC20 value of CU-O75 at 12 and 24h

In vivo studies. Mouse xenograft models were previously described¹. Briefly, 10^{10} HBL-1 and OCI-Ly1 cell lines were injected subcutaneously to flanks of 4-6-week-old SCID beige mice (n=10 per group). Once the tumors were visually observed, they were measured and when they approached 55 mm^3 , mice were randomized into treatment groups, either DMSO control or the NQBS treated ones. Volumes were measured every 3 days. Mice were sacrificed if tumor volumes exceeded 2000 mm^3 . This study was undertaken in accordance to Columbia University's IUCAC approved protocol.

We also used genetically engineered transgenic mouse (n=3) using a CherryLuciferase fusion gene targeted to the CD19 locus to achieve B-cell–restricted fluorescent bioluminescent emission in transgenic mouse models of living mice as previously described^{Error! Bookmark not defined.}. This study was undertaken in accordance to New York University's IUCAC approved protocol.

Statistics. IC50 (half the maximal inhibitory concentration) for each cell line was calculated using the CalcuSyn Version 2.0 software (Biosoft, Cambridge, UK). The Wilcoxon rank-sum test was used to calculate the statistical significance *in vivo* for both actual and relative tumor volume. Relative tumor volume was calculated by comparing the actual volumes divided by the volumes on day 1 between the groups. A global test for significance was conducted by calculating the area under the actual (or relative) tumor volume curves using the trapezoidal rule.

Supplemental References

Jafari R, Almqvist H, Axelsson H et al. The cellular thermal shift assay for evaluating drug target interactions in cells. *Nat Protoc.* 2014;9:2100-22.

Kalac M, Scotto L, Marchi E et al. HDAC inhibitors and decitabine are highly synergistic and associated with unique gene expression and epigenetic profiles in models of DLBCL. *Blood.* 2011; 118:5506-16.

Neves MAC, Trotov M, Abagyan R. Docking and scoring with ICM: the benchmarking results and strategies for improvement. *J Comput Aided Mol Des* 2012; 26:675–86.

Subramanian A, Tamayo P, Mootha VK et al. Gene set enrichment analysis: A knowledge-based approach for interpreting genome-wide expression profiles. *PNAS.* 2005;102:15545-50.

Woo Hoon J, Shimoni Y, Yang WS et al. Elucidating Compound Mechanism of Action by Network Perturbation Analysis. *Cell.* 2015;162: 441–51.